Light conversion materials for solar cells by atomic layer deposition

by

Per-Anders Hansen

A thesis submitted for the degree of
Philosophiae Doctor (Ph.D.)

Department of Chemistry
Faculty of Mathematics and Natural Sciences
University of Oslo

March 2014

Series of dissertations submitted to the
Faculty of Mathematics and Natural Sciences, University of Oslo
No. 1497

ISSN 1501-7710

Cover: Inger Sandved Anfinsen.
Printed in Norway: AIT Oslo AS.

Produced in co-operation with Akademika Publishing.
The thesis is produced by Akademika Publishing merely in connection with the thesis defence. Kindly direct all inquiries regarding the thesis to the copyright holder or the unit which grants the doctorate.

Abstract

There are many different solar cell technologies which aim at producing electricity from sunlight cheap and/or efficient. As the efficiency of silicon cells is slowly but continuously climbing, price plummeting, and production skyrocketing, there is in my opinion little room for other technologies unless they can beat silicon on efficiency. Commercial cells at over 20 % efficiency are available and lab cells have been reported at above 27 %. Comparing this to the theoretical maximum efficiency of a single junction cell which is just above 30 % shows that we are able to produce close-to-perfect silicon cells. Any technology which wants to beat this has to aim at an efficiency higher than 30 %. There are not per today many potential candidates for this.

One aspect that often seems to be overlooked is what exactly 20 % efficiency means for a solar cell. For regular off-the-shelf silicon cells, this efficiency is a combination of zero efficiency at > 1100 nm, more than 70 % in the 700 – 1000 nm range and steadily decreasing efficiency towards the UV. That means that if we could convert all the solar *energy* to 1000 nm light, the efficiency of solar cells would be drastically increased without changing the cell itself. Unfortunately we do not know how we would do this today, but we know a few steps on the way there. Down and up conversion aims at splitting one UV photon into two lower energy photons and merging two low energy photons into one medium energy one, respectively. This would in theory double the solar cells efficiency in the UV range and enable the cell to utilize the > 1100 nm light.

This work is part of work package 4 *New materials for next generation solar cells* (WP4) in *The Norwegian Research Centre for Solar Cell Technology* (FME-Sol). The objective of this thesis is to build competence in the field of light conversion and to attempt at making an efficient down conversion film material by atomic layer deposition (ALD). This has resulted in four papers, two which are yet to be published. In addition, a significant part of the work has

been devoted to popularization of science through lectures to non-scientific audiences.

The potential down conversion materials that exists in the literature usually depends on the interaction between several different types of atoms and often with the host material itself as the UV absorbing material. As ALD grows the film one sub-monolayer at a time, it can give some quite unique control over the atomic distribution throughout the film. It is relatively easy to switch between several different cation cycles at will through the deposition which enables mixing of atoms that would separate or form precipitates under other conditions in addition to the ability to have some control of the next-neighbor distribution around each type of atom.

Europium titanium oxides were chosen as the model system for this investigation. This system has the characteristic luminescence of Eu^{3+} and strong UV absorption of TiO_2. Both binary oxides are relatively easy to synthesize by ALD. Thin films of both Eu^{3+} doped anatase and amorphous $Eu_xTi_yO_z$ was deposited, while crystalline $Eu_2Ti_2O_7$ was obtained through annealing. In addition to homogeneous mixing, sandwich structures of separated Eu_2O_3 and TiO_2 layers were deposited. Thus, this system provides a good opportunity to investigate the relationship between the luminescence of the material and the concentration, local symmetry and interatomic arrangement and distances.

The final stage of this thesis was to attempt to make a down conversion material by replacing Eu^{3+} with Yb^{3+}/Ln^{3+}. These lanthanide pairs have been reported in literature to split one high energy excited state into two lower energy excited states. In this work, energy transfer and luminescence was observed, but efficient down conversion was unfortunately not obtained. However, ALD was shown to enable some control of the arrangement of the cations which could lead to down conversion in other material systems which are not easily obtainable by other routes.

Acknowledgements

When I finished my master's degree I knew that I wanted to do research in new materials or concepts for solar cells, and I can't complain about the timing. The same year as I finished my master's defense, the Norwegian Research Centre for Solar Cell Technology was started. Several PhD positions appeared at UiO and IFE, one of them being about reshaping the sunlight for solar cells. That did indeed sound awesome, and just a few months after I was ready to start.

When I started this work, I had very little knowledge about luminescent materials. I would like to thank my supervisors, Ola Nilsen, Helmer Fjellvåg and Terje Finstad for the freedom I have had to explore what I feel is important and go where I think I will learn something. There were many gaps in my knowledge about luminescence that the courses at UiO could not fill, and being able to go to two international and one national summer school have been crucial for my understanding. What courses and books could not answer I have tried to test experimentally. When I couldn't find the ingredients I needed in the lab, they tended to magically appear in the lab a few weeks after talking to my supervisors. Without this freedom to explore I would definitely not have the same understanding of luminescent materials as I have today.

I also had the great opportunity to participate in Researcher Grand Prix during UiO's 200 years celebration, were participants have only 4 minutes to make their science project interesting and entertaining to a non-scientific audience. There I learnt a lot about conquering stage fright and how to keep things simple and short, which have been a great help for science conferences and such later. Afterwards I have also gotten the opportunity to do plenty of popular science lectures for various audiences which have been a lot of fun, and surprisingly educational. I learnt that you don't really understand something before you can explain it to someone else. When preparing popular science lectures I often had to stop and think "Wait, this doesn't make sense" and start re-reading books and articles. Truly, knowledge comes from discussion and sharing of ideas, not working alone in the lab or office.

I would also like to thank the other students and researchers at the Nafuma group, and also the MENA students and their (sometimes) semiannual cabin trips, for making these 4 years a fun and social experience. It's the small things that make life good, and sharing a laugh and venting of frustration around the lunch table makes a good break from work. You have been a nice and varied group of people, ranging from serious and hardworking to the fun and playful and the kind and gentle. Especially I would like to thank my office mate Knut Bjarne Gandrud who has spent the last 4 years distracting me with games and miniature battles. Good luck now that it's your turn!

Lastly I would like to thank my family, friends and my girlfriend Marie-Pierre. You have all been supportive, interested when I try to explain what I do and have done a very good keeping me motivated for my work. I am very grateful for having each and every one of you!

Table of contents

Chapter 1 – Introduction

1.1 The energy challenge

Among the large challenges facing humanity, a secure energy supply to the world's economy and society is one of the largest. In addition many of the other major challenges, like food, clean drinking water and poverty is either directly or indirectly related to the energy challenge. The IPCC's newly published report on the physical science basis for climate change shows with clarity the impact that our society and industry has on our climate and how that in turn will have strong negative impacts back on us [1]. An easier to read summary of the over 2000 page document is also available [2]. It is beyond doubt that fueling our economy and society with fossil fuels is very detrimental to both on the long term. A crucial part to mitigate climate changes and securing a pollution free energy supply is a large scale switch to renewable energy sources [3].

From the media, it can seem like there is a technological barrier to the large scale switch to renewables like wind and solar and that a breakthrough of some kind is needed. In fact, the technologies we have available today are in fact sufficient, while the bottleneck is rather the policies and economic incentives to implement it [4, 5]. One major obstacle for renewables is that the competing fossil fuels are also subsidized and reducing these subsidies is difficult due to the large invested interests in these industries [3]. In addition, fossil fuel subsidies are complex, numerous and not always easily identified making it hard to estimate it on a global level [6]. It is thus wrong to argue that renewables "relies on subsidies", as all types of power generation is in fact subsidized in one way or another [7]. In particular photovoltaics is often claimed to need a breakthrough in either cost or efficiency in order to be competitive. It is argued in a recent paper that this conception is both misleading and out-of-date [8]. The authors also argue that this misconception

among policymakers is detrimental to the implementation of policies and investments for the large scale use of PV. On the bright side, changes are happening. According to a REN21 report [9], "*renewables accounted for almost half of the estimated 208 gigawatts (GW) of electric capacity added globally during 2011. Wind and solar photovoltaics (PV) accounted for almost 40% and 30% of new renewable capacity, respectively, followed by hydropower (nearly 25%)*".

Of all the energy resources available to us, including the non-renewables, solar energy is by far the largest. Despite all the misconceptions and policies favoring fossil fuels, countries around all over the world are implementing many different incentive schemes and policies in order to increase the use of solar energy [10] and photovoltaics [11]. To put solar energy in perspective, the amount of solar energy hitting our planet is roughly 10.000 times our total energy usage. This number is only for illustration though as it would require the use of every square centimeter of the earth with 100 % efficiency. A more technical potential, using more realistic conversion efficiencies and land areas, is still between 3 – 100 times the worlds primary energy need[*] as of 2008 [12]. In addition, the environmental impact of solar energy technologies is low, even compared to other renewables like wind and hydro [13].

Photovoltaics has arguably been the largest growing form of renewable energy the last years, much due to Germanys ambitious investment in PV followed by China. According to the REN21 report quoted earlier "*Solar PV grew the fastest of all renewable technologies during the period from end-2006 through 2011, with operating capacity increasing by an average of 58% annually*" [9]. An overview of the world market, production and outlook of photovoltaics can be found in the PV Status Report 2012 [14]. Around 90 % of solar cells today are silicon based technologies, and the price of PV electricity was dominated by the silicon prices. This price has decreased enormously over the last decades making the cost of the cell itself only about ⅓ of the total price of a PV installation. Even though a lot can be done to further reduce the cost of cell production, more and more focus is now given to increasing the efficiency of solar cells. In short, a small increase in efficiency will have a larger impact on the total cost of PV than a decrease in production cost of the cell.

To summarize this a bit, solar energy is by far the largest energy resource we have and PV is an excellent way to harvest it. In order to continue the

[*] Total energy input needed from energy sources like solar, wind and fossil sources.

exponential growth of PV we have to work on better policies and incentives to invest in PV and to increase the efficiency of the solar cells. The latter is where we material scientists can contribute.

1.2 Solar cells

To have an idea of how to improve the efficiency of solar cells, we first need to understand how it works and why it is not 100 % efficient in the first place. The description in this chapter is highly simplified, but should be enough for the discussion in this thesis. A much more thorough description of solar cells can be found in the textbooks by P. Würfel [15] or M. A. Green [16]. For readers who are relatively new to the field of solar cells and semiconductor physics, the textbook by J. Nelson may be more approachable [17].

When photons are absorbed in a material, an electron gets excited to a higher energy state. The aim of a solar cell is to extract this electron and convert its energy to electricity. In order to do this, two things are required by the material. First, the excited state (also called a conduction band, E_c) must be separated (in energy) from the ground state (also called a valence band, E_V) by a forbidden band gap E_g. This prevents the electron from immediately relaxing back to the ground state, giving it some time[*] to stay in the excited state. Second, the excited electron needs to be separate from the hole left behind in the ground state. Although there are more ways to accomplish this, most solar cells accomplish this separation with a p-n junction.

When an n-type and p-type material comes in contact, a so called depletion region is formed at the interface and stretches some distances into the doped regions. Inside the depletion region, there is an electric field pointing from the n-type to the p-type region. If an electron gets excited to the conduction band in this region, it will be pulled towards the n-type region by the electric field. The hole which is left behind in the valence band will likewise be pulled towards the p-type region. The electron and hole are physically separated and prevented from getting back together by the electric field across the p-n junction. Electrons collected this way, or generated in the n-type region, will contribute to an electrical current through an external load, giving us electrical power. This is illustrated in Figure 1.

[*] Usually in the ns or µs range. Longer is better for solar cells.

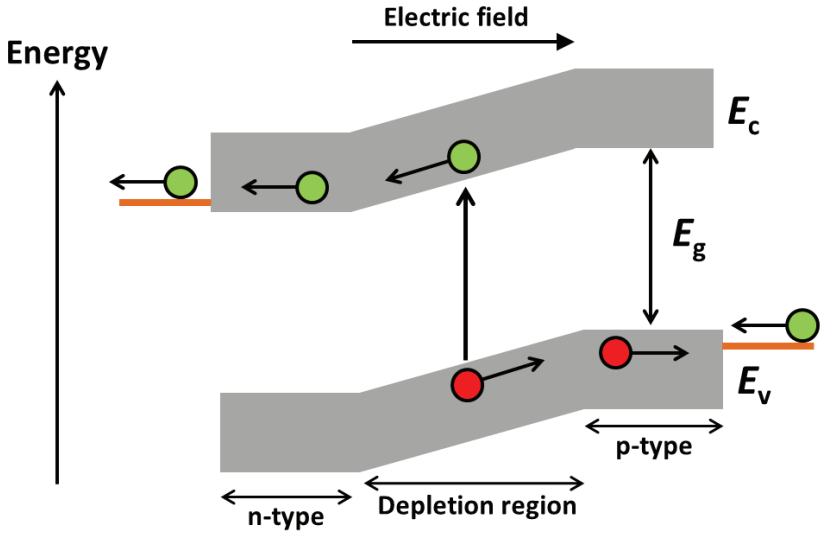

Figure 1: An illustration showing an electron being excited from the valence band to the conduction band. The electron is then pulled towards the n-type region and the hole is pulled towards the p-type region.

The band gap is crucial in order to let the excited electron maintain its energy. Unfortunately, it also puts strong limitations on which parts of the solar spectrum the cell can utilize. If the energy of the photon, E_λ, is smaller than E_g, the photon cannot excite an electron from the ground state to the excited state, and therefor will not contribute anything to the electrical current generated. On the other hand, if E_λ is larger than E_g then the excited electron will quickly relax down to the lowest allowed energy in the excited state. The surplus energy will be released as phonon so the energy is lost as heat. This process is called thermalization. The sunlight consists of photons with vastly different energies, as shown in Figure 2. The band gap of silicon is 1.1 eV which corresponds to a photon of 1100 nm wavelength. That means that all the photons with longer wavelengths cannot be utilized to generate power, while for photons of shorter wavelength the thermalization loss increases rapidly with decreasing wavelength. For silicon, this means that about 1/3 of the energy of the sunlight consists of too low energy photons to contribute and 1/3 of the energy of the high energy part of the spectrum is lost as heat, putting the theoretically highest efficiency at just over 30 %. This is also called the Shockley-Queisser limit [18].

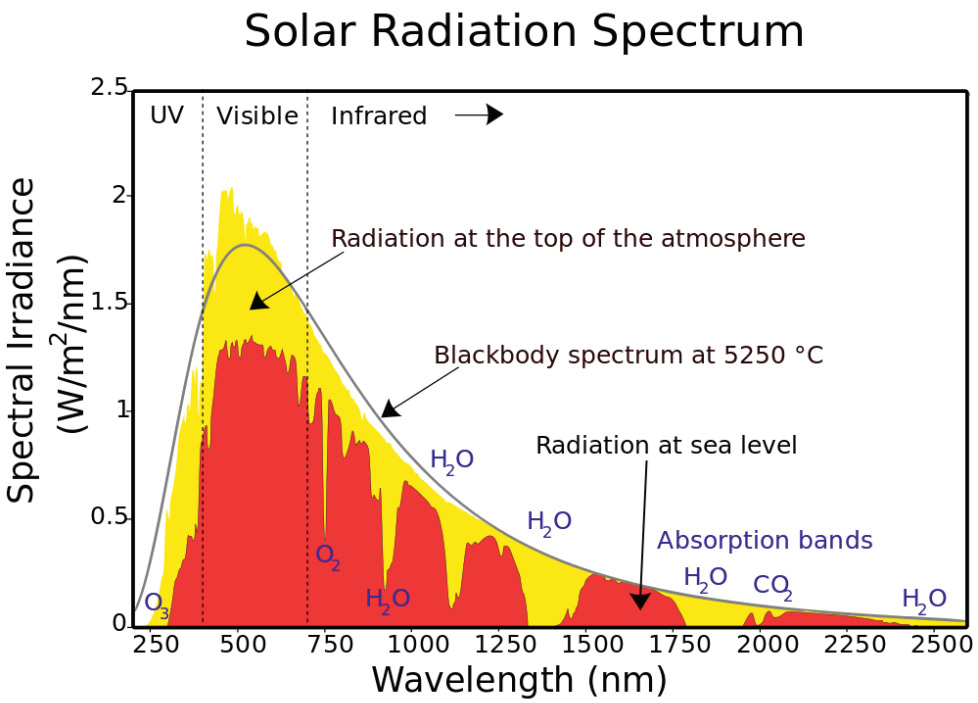

Figure 2: The solar spectrum showing an ideal blackbody spectrum (black curve), the solar spectrum reaching the top of our atmosphere (yellow) and the solar spectrum reach ground level after some absorption through the atmosphere (red). Image adopted from Wikimedia Commons [19].

So, how well do actually solar cells convert solar energy into electricity? The National Renewable Energy Laboratory in the US have a continuously updated graph * showing the record efficiencies of different solar cell technologies [20]. The lab record for non-concentrated silicon solar cells have been 25 %, set by Green *et al*. with a PERL† cell [21]. Just recently in April this year, Panasonic broke this record with a 25.6 % efficient HIT‡ cell [22]. Commercial silicon solar cells can reach efficiencies above 21 % [23]. As the theoretical limit for a single junction solar cell is about 30 %, this means that silicon solar cells are close to perfect. This, along with the fact that solar cells

* This is a large graph that is better viewed on a computer screen than in a text page.
† Passivated Emitter, Rear Locally diffused (PERL).
‡ Heterostructure with Intrinsic Thin film (HIT).

are becoming commercially competitive more and more places, leads us to a few conclusions:

1. Silicon solar cells can be made cheaper, but not drastically more efficient than they are today.
2. The two major obstacles to higher efficiencies are a) the thermalization losses of the high energy photons and b) that the sub band gap photons cannot be used.
3. Neither of these obstacles can be overcome when combining a single junction solar cell with the solar spectrum.

If we are to make solar cells that are substantially more efficient than they are today, we are left with two options. The first option is to replace the single junction cell with multi junction or tandem cells, which are usually made from III-V semiconductors[*]. This has been remarkably successful with respect to efficiency, with several labs around the world producing cells with efficiencies above 40 %. Unfortunately, these cells are very difficult and very expensive to make. They are useful only in concentrator systems where they are prone to sudden overheating, making them much less reliable than conventional large area single junction cells. The second option is to adapt the solar light to better fit the single junction cell. Compared to the multi junction cells, this has been much less successful so far.

1.3 Luminescence for solar cells

Luminescent materials can be used for solar cells in three ways. First, down shifting (DS) UV and blue photons can bypass the poor quantum efficiency that some solar cells have in this range. Second, luminescence can be used to concentrate light in what is called luminescent solar concentrators. Third, down conversion (DC) and up conversion (UC) can be used to avoid the losses due to thermalization and sub band gap photons.

The possible gains from down shifting high energy photons is discussed by E. Klampaftis *et al.* in a review paper from 2009 [24]. A solar cell with high

[*] These are materials made from elements in group III (Al, Ga, In) and V (N, P, As) in the periodic table. By gradually changing the composition, it is possible to change the bandgap from 0.35 eV (InAs) to 6.2 eV (AlN).

quantum efficiency in the visible range and poor efficiency in the UV/blue range can benefit the most from down shifting. Figure 3 shows the external quantum efficiency * (EQE) for several technologies. This type of light conversion has the highest potential for CdTe and CIGS which uses CdS buffer layers in front of the cell which blocks the UV and blue light. For Si technologies, both mono- and multicrystalline Si cells often have high EQE's in the blue range as well, limiting the potential to the UV range. Some enhancement is possible, however. One example is Chen *et al*. which observed an increase in efficiency of a Si cell from 17.1 % to 17.7 % by adding a down shifting layer [25].

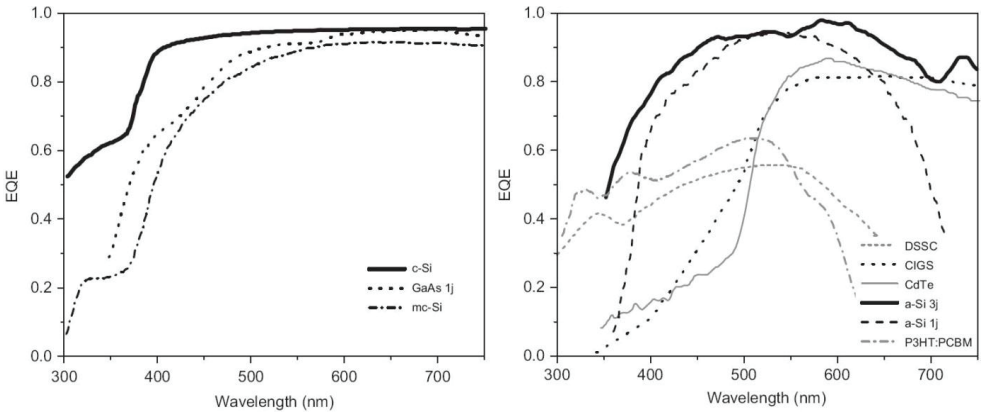

Figure 3: External quantum efficiencies in the UV-Vis range for several solar cell technologies. Reproduced from [24].

Down conversion on the other hand will benefit all types of cells. By splitting one high energy photon into two lower energy photons, such materials could in principle increase the quantum efficiency of a cell up to 200 % in the UV and blue range and reduce the thermalization losses. Trupke *et al*. investigated theoretically the use of a DC layer in the front surface of a solar cell [26]. They found that the maximum possible efficiency of that design was 39.6 % for E_g = 1.05 eV and 38.6 % for Si (E_g = 1.1 eV), assuming a DC quantum efficiency of 200 % and including the loss from some of the DC luminescence being emitted out from the cell. This is a significant improvement over the maximum 30.9 % efficiency of a solar cell without a DC layer under the same

* EQE is how many electrons are extracted per photon incident on the solar cell surface, including all optical losses like reflection.

conditions. Richards discusses some of the possible DC mechanisms which are relevant for solar cells in a paper from 2006 [27]. He concludes that while in theory DC has potential, the EQE of the DC layer needs to be well above 100 % in order to compensate for some of the emission going out of the cell and that there aren't many concepts that are likely to have a high enough EQE. Yb^{3+}, however, comes out as a potentially promising candidate as it only emits light around 1000 nm, ideal for Si cells. There are also several pairs of lanthanides which seem to show the potential for DC, like Tm^{3+}/Yb^{3+} and Tb^{3+}/Yb^{3+}. Zhang *et al*. gives a thorough overview over the materials and mechanisms that show DC, both for lighting and solar cells, in a paper from 2009 [28]. In this paper, it is apparent that in both cases the majority of potential DC materials are in fact lanthanide based.

Up conversion will also benefit all types of solar cells, as sub band gap photons are not used at all. Compared to DC which has to be more efficient than the EQE of the solar cell, even low efficiency UC is interesting from an efficiency point of view. Trupke *et al*. published a theoretical model of an ideal solar cell under 6000 K black body irradiation in 2002, showing a maximum efficiency of 47.6 % for a solar cell with a band gap of 2 eV and an ideal UC layer [29]. This work was extended to include the AM1.5 spectrum in 2006 [30], which showed a maximum efficiency of 50.6 % for a 2 eV band gap, and about 39 % for 1.1 eV. Shalav *et al*. published in 2007 a paper describing the UC mechanisms relevant for solar cells [31]. This paper had a special focus on UC in lanthanide based systems, and in particular on $NaYF_4:Ln^{3+}$. They conclude that UC by lanthanides is possible, but a major obstacle is the very high intensity required to increase the UC efficiency along with the narrow and weak absorptions spectrum of the lanthanides. Other non-lanthanide UC processes also exist that can provide high conversion efficiencies, like triplet–triplet annihilation (TTA) in organic materials [32] and second harmonic generation in non-linear crystals. Unfortunately, most of these processes either convert light which is already well suited for solar cells or require intense laser pulses to be efficient. Both UC via lanthanides [33-35] and TTA [36] have been tested on solar cells and shown to give an improvement. However, the improvements of the efficiency of the total cell have been minor.

In summary, DS can most easily be implemented as highly luminescent materials are available. However, this cannot increase the Shockley-Queisser

limit. DC and UC on the other hand can do this. In both cases, the most efficient reports are on lanthanide based systems, for either DC of <500 nm light or UC of >1100 nm light. Ende *et al*. summarizes the literature available regarding the use of lanthanides for up and down conversion for solar cells [37]. For DC, there are many reports of one excited state splitting into two lower excited states with very high efficiency. These systems still often show poor luminescence. Either the lower lying levels relax non-radiatively or there is a poor energy transfer from the UV/blue absorbing host to the higher energy lanthanide level. At high lanthanide concentrations, cross relaxation is also often observed which quenches the luminescence. For UC with lanthanides, the major obstacle is the narrow and very low absorption. This makes it difficult to obtain a high concentration of excited states without using light intensities far higher than what is possible with even concentrated sunlight. For both DC and UC the potential is definitely there, but some major challenges have to be solved before this can be utilized commercially for solar cells.

1.4 Motivation for this work

As the challenge for DC materials seems to be the interaction between the different types of atoms, control of the spatial distribution and local symmetry around these atoms is crucial. We believe that atomic layer deposition (ALD) offer a unique control of the film material in this respect. As the films are grown one sub-monolayer at a time, it is possible to have very precise control of the atomic distribution in the film growth direction [38]. In addition, each precursor molecule takes up a certain amount of surface area during growth. Thus it should also be possible in some cases to have control over the distribution in the film plane by controlling the shape and size of the precursor molecules. Lastly, since the films are grown at relatively low temperatures, it is often possible to grow amorphous films [39] whose crystallinity can be modified ex-situ by for example annealing [40]. It has also been shown that in some cases, the film material will adopt the same or similar crystal structure as that of the substrate [41, 42]. It is thus possible to grow crystal phases that are metastable or otherwise difficult to obtain by other techniques.

The motivation of this work is to explore how the layer-by-layer and low temperature growth affects the optical and luminescence properties of the film

materials. In the long run, the aim is to use the control that ALD offers to improve the interactions between the different types of atoms in lanthanide based down conversion systems.

Chapter 2 – Theory of optical properties of ions in materials

The majority of phosphor materials used today is based on the luminescence from single ions in a host material, often an oxide. For down conversion systems, the interaction between different lanthanides ions or the interaction between lanthanide ions and one or more other ions, like transition metals, is the most common strategy. Thus, as this thesis focus on lanthanide based down conversion systems, we need to understand how ions interact with photons, and how excited ions interact with other ions. In this chapter, the basic theories of the optical properties of ions in materials are explained.

Photons can have a very large range of energies, or wavelengths. This ranges from very low energy long radio waves through infrared (IR), visible light (Vis), ultraviolet (UV), X-rays, γ-rays and more or less up to infinity. The spectrum of the sunlight lies somewhere in the middle[*], ranging approximately from 250 – 2500 nm (see Figure 2). The topic of this thesis is light conversion for solar cells, thus light in this context will refer to photons in the range defined by the sunlight.

[*] The middle between zero and infinity is in fact not very well defined, but let's assume it includes the solar spectrum.

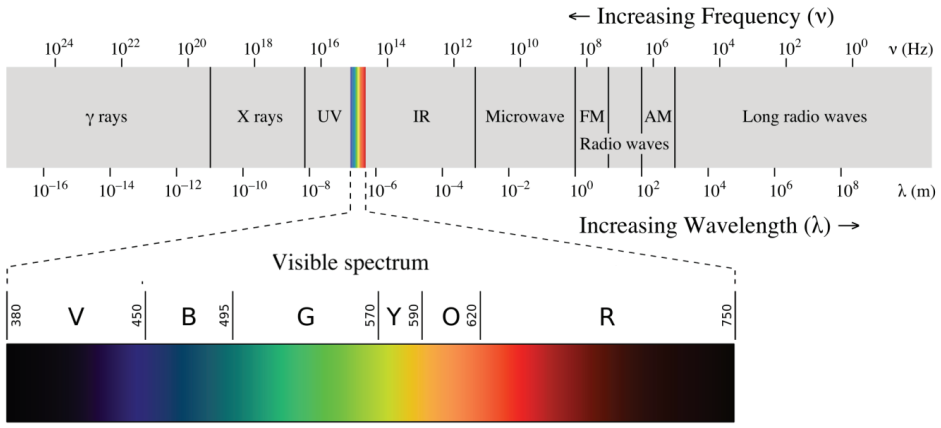

Figure 4: The electromagnetic spectrum, showing the small portion we call visible light (380 – 750 nm). Image adapted from Wikimedia Commons [43].

2.1 Absorption of light

Photons can interact with material in several ways, but in the range relevant in this thesis (250 – 2500 nm) the dominant interactions are absorption through electronic transitions, refraction, and reflection due to the refractive index of the material*. An electronic transition means that an electron in an (occupied) energy state absorbs the energy of the photon and gets excited to a higher energy unoccupied state. This higher energy state can also be situated on a neighboring atom, in which case both atoms change oxidation state in a process called charge transfer (CT). This requires that there exists an occupied state and a higher energy unoccupied state with an energy difference exactly the same as energy as the photon. Thus, absorption of light can be very wavelength specific. This is well illustrated by the ruby in Figure 5. The red color comes from strong and narrow absorption of green and blue (and UV) light while being transparent to red and IR light.

* This also applies to liquids and gasses as well. In fact, this strictly applies to any volume of anything, including vacuum.

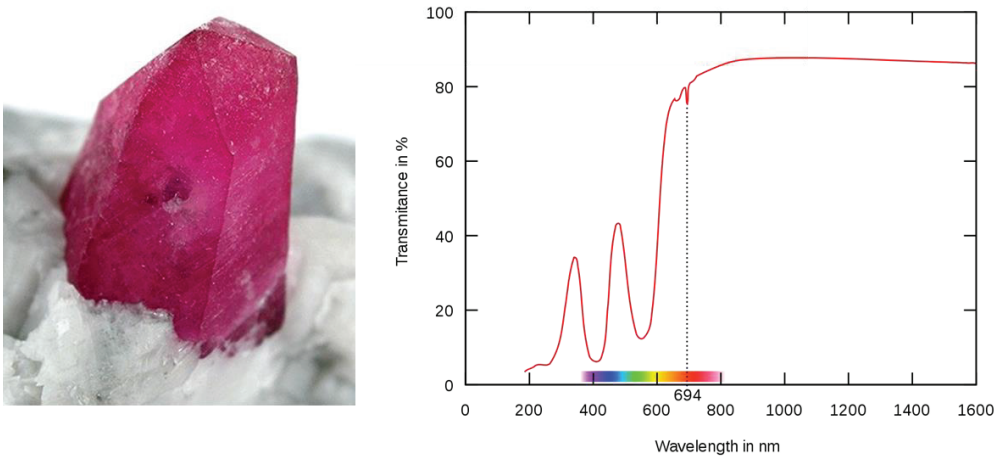

Figure 5: The red color of a ruby (left) coming from strong absorption of blue and green light (right) [44, 45].

Semiconductors like Si and GaAs are characterized by an absorption edge, where photons of lower energy are transmitted and those of higher energy are absorbed. This strong and broad absorption stems from transitions between delocalized states in the filled valence band and empty conduction band, separated by a bandgap E_g. Many materials, in particular those who contain transition metals or lanthanides, can have weak or strong absorption peaks in addition which comes from electron transitions between states localized on a single atom. The specific transition dominating in the color of the ruby involves an electron in the valence d-shell of the Cr^{3+} impurities in the corundum (Al_2O_3) crystal being excited from its ground state to a higher energy d-orbital.

2.2 Refractive index *n* and attenuation coefficient *k*

All materials have a refractive index and an extinction coefficient. Even though the words index and coefficient indicates that these are simple numbers, both are in fact functions depending on the wavelength of light and should strictly be written $n(\lambda)$ and $k(\lambda)$ instead of n and k. The latter is often used for simplicity though and is found in many textbooks and publications as the wavelength of interest is usually visible light (380 – 750 nm) and transparent materials usually have little variations in $n(\lambda)$ and $k(\lambda)$ in this range. In short, $n(\lambda)$ describes how

much light is slowed down in the materials while $k(\lambda)$ describes how strongly it is absorbed. The relation between $k(\lambda)$ and the absorption coefficient $\alpha(\lambda)$ is given by Eq. 2.1.

$$\alpha(\lambda) = \frac{4\pi}{\lambda} k(\lambda) \tag{2.1}$$

$n(\lambda)$ and $k(\lambda)$ is in turn related to each other through the materials dielectric function $\varepsilon(\lambda)$. The relevant part to this work is that $n(\lambda) = 1$ if $k(\lambda) = 0$ for all wavelengths (i.e. vacuum) and that an absorption at wavelength λ_0 affects $n(\lambda)$ at all wavelengths. This is illustrated in Figure 6. The idealized material shown here has a single absorption peak in the yellow part of the spectrum, which affects $n(\lambda)$ in the whole spectrum. From the IR part, $n(\lambda)$ increases towards the absorption peak, then "turns" around the absorption itself. If there had been an absorption peak in the deep UV, $n(\lambda)$ would again start to increase towards it. All materials absorb light in the deep UV, even those that are otherwise transparent. A material that absorb near UV (300 – 400 nm) light will have a steeper increase in $n(\lambda)$ in the visible range. Thus UV absorbing materials like diamond, TiO_2 and ZnO have high $n(\lambda)$, while UV transparent materials like silica, Al_2O_3 and MgF_2 have low $n(\lambda)$.

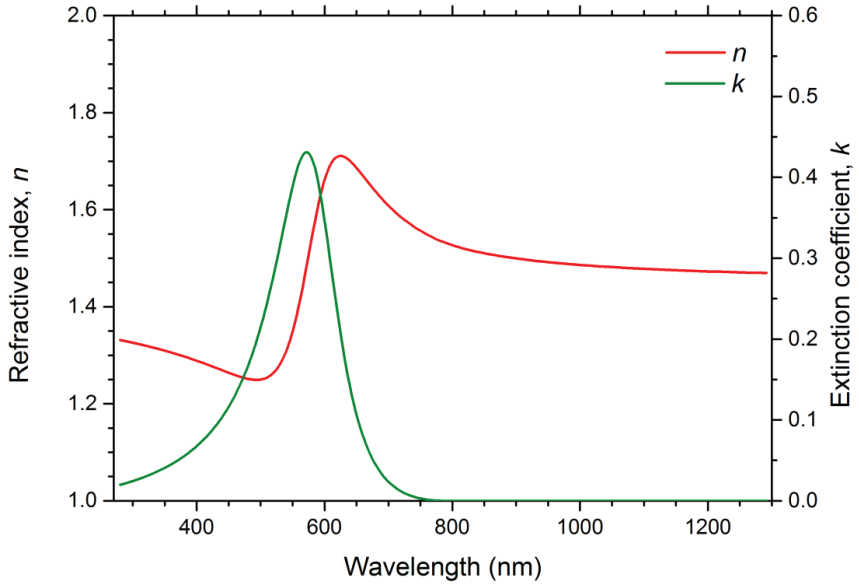

Figure 6: The refractive index increases with decreasing wavelength in the transparent part (λ > 800 nm) and "turns" at the absorption peak.

2.3 Luminescence

Luminescence is the opposite of the absorption. Instead of an electron being excited by the absorption of a photon, an excited electron relaxes to a lower energy unoccupied state (sometimes the ground state) by the emission of a photon. Again, a ruby illustrates this process. In Figure 7, the synthetic rubies to the left are lit by normal fluorescent room light and the red color is visible due to the absorption of the green and blue part of the light. The same rubies are shown on the right illuminated by monochromatic green light. The rubies still appear red, even though no red light is present in the light source. The red light comes from the relaxation of an electron which was excited by the absorption of the green light.

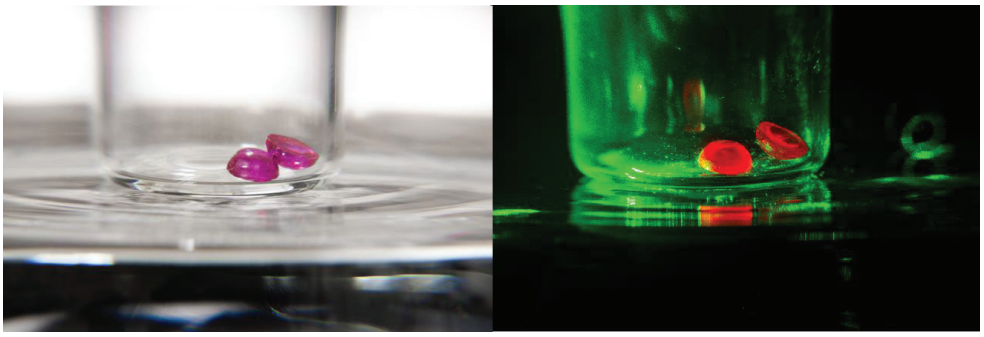

Figure 7: Synthetic rubies under fluorescent room light (left) and monochromatic green light (right) [46, 47].

Luminescence is used extensively in our modern society and is a major field in research. There are several review articles summarizing the field in general and specific subcategories, for example for lighting and displays [48] and for d-metal coordination compound [49].

2.4 Atomic energy states

For both absorption and luminescence to be possible, an atom needs to be able to exist in different states with different energies. These different states can for example arise from the addition or removal of an electron from an atom, or a rearrangement of which orbitals are filled. The transfer of an electron from one atom to another is called a charge transfer (CT). It usually requires relatively much energy to do this, and the absorption and emission from such states mostly lie in the UV or VUV range. The rearrangement of electrons within the orbitals of the same atoms on the other hand doesn't necessarily require much energy, and these states can span the entire range from NIR to VUV. Most non-semiconductor materials that luminesce in the visible or NIR range are in fact based on simple rearrangement of electrons within the same atom.

Transition metals and lanthanides can have partially filled d and f shells where the electrons can be internally rearranged to form states of different energies. A transition from one d state to a different d state is called a d → d transition, and similar for f → f transitions. The energy of the excited states and the transition between them is governed by the same rules for the f and d orbitals. The reasons why the difference is so large in the line width, lifetimes,

absorption strength and emission efficiencies between d → d and f → f transitions is largely due to the shielded nature of the f-shell and the spin-orbit coupling of the f-orbitals. As most university courses focuses on transition metals, I feel that it is useful to compare the f states of the lanthanides with the d states of the transition metals to understand how the nature of the f-shell give rise to the optical properties of the lanthanide ions.

The color of a transition metal in a specific oxidation state, say the d_3 ion Cr^{3+}, can vary a lot from compound to compound and solution to solution. The differences originate from how the surrounding atoms push and pull on the d orbitals, called the crystal field. When the surrounding atoms push on the orbitals of the central atom, some of these orbitals will have a change in symmetry and energy. For example, when an atom is octahedraly coordinated, two of the d orbitals (d_{z^2} and $d_{x^2-y^2}$) will point directly at the neighbouring atoms, Figure 8. An electron in one of these orbitals will then be closer to the electron cloud of the other atoms, compared to the other three d orbitals (d_{yz}, d_{xy} and d_{xz}). These two orbitals will thus feel a greater electrostatic repulsion and lie higher in energy than the other three orbitals. However, as an octahedral coordination is centrosymmetric, each of the 5 orbitals still have the same symmetry. If the atom is in a non-centrosymmetric environment, like in a tetrahedron, the push and pull on the d orbitals will distort the symmetric shapes of the orbitals as well. This has the effect of lifting the Laporte selection rule, which states that transitions between orbitals of the same symmetry are forbidden, making the transition rates between different states greatly enhanced in non-centrosymmetric surroundings. Thus, solutions and crystals containing tetrahedrally coordinated d-metals are more strongly colored than those containing the same element octahedrally coordinated.

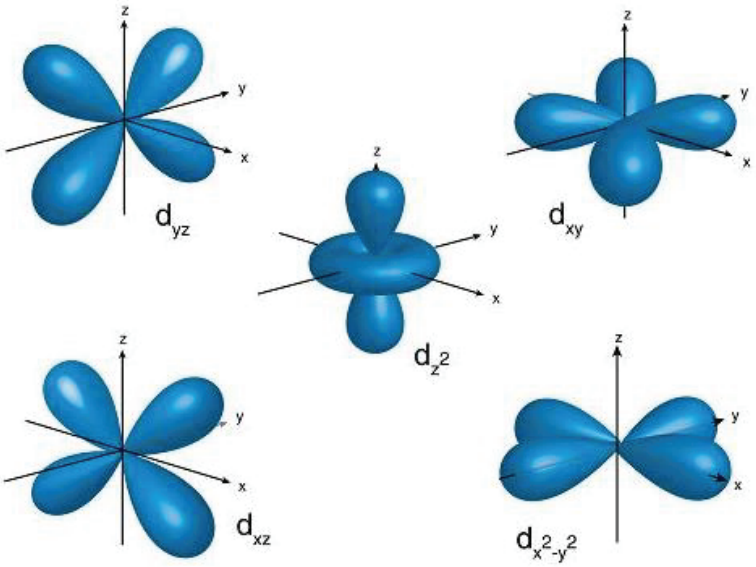

Figure 8: The shape of the 5 d orbitals.

The second important rule governing the transition rates between states is the spin selection rule which states that transitions between states of different total spin are forbidden. Taking the d_3 ion Cr^{3+} as an example, we know from Hund's rule that the ground state will have three unpaired electrons. The two lowest excited states are illustrated in Figure 9. One transition is spin forbidden and the other spin allowed, while both are Laporte forbidden. The spin allowed transition will cause a much stronger absorption than the spin forbidden.

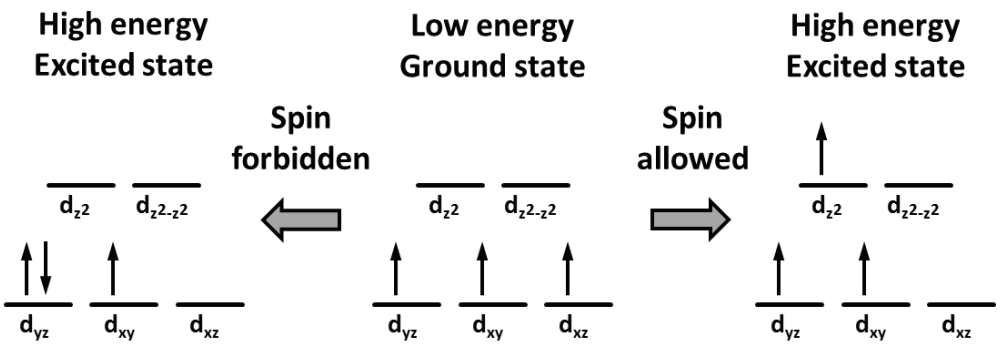

Figure 9: A low energy state with a total spin S = 1/2 (left) and high energy state with S = 3/2 (right).

The last important aspect of optical absorption and emission in atomic systems like these are illustrated by the configurational coordination diagrams, as in Figure 10. Without a surrounding crystal field, each orbital in the same shell have the same principal quantum number and the same average distance between the electron and the nucleus. When the crystal field pushes some of the orbitals closer to or further from the core, the orbitals no longer all have the same average distance to the core and not the same momentum. Thus, the excited state on the right in Figure 9 differs from the ground state in both momentum and energy, which both needs to be conserved during an absorption or emission of a photon.

A photon does not carry a momentum. The change in momentum has to come from something else. This momentum change often comes from the absorption or emission of phonons, which carry momentum in addition to a relatively small amount of energy (compared to the photon). When transitions between states of different momentum occur, the final state is vibrationally excited in order to preserve momentum. At temperatures above zero kelvin, the initial state may also be vibrationally excited. After the optical transition, the vibrationally excited final state will relax by the emission of phonons. This is illustrated in Figure 10. As a result, the emitted photon has a different energy than the absorbed photon. This energy difference is called a Stokes shift if the emitted photon has less energy, and anti-Stokes if it has more (meaning some phonons were absorbed during the process).

At higher temperatures, the initial state has a higher probability of being vibrationally excited. This has the effect of broadening the absorption and emission peaks as there now exist a small range of possible vertical transitions. In addition, this can cause temperature quenching. At higher temperatures, the excited state will also be more and more vibrationally excited. The small range of vertical transitions down to the ground state now includes some smaller energy gaps. An energy gap between two states can be crossed by the emission of phonons instead of a photon. As a rule of thumb, phonon emission dominates over photon emission if the energy gap is less than 6 times the maximum phonon energy in the material. Thus, as the temperature increases, smaller and smaller energy gaps will be available, meaning more of the excited states will relax by phonon emission instead of photon emission and the luminescence is effectively quenched (illustrated by the grey arrow in Figure 10). The larger the difference in momentum is, also meaning the stronger and more unevenly the orbitals are pushed upon by the surroundings, the stronger effect has this temperature quenching. For f – f transitions that have virtually no momentum difference, the luminescence can be efficient up to several hundred degrees Celsius [50].

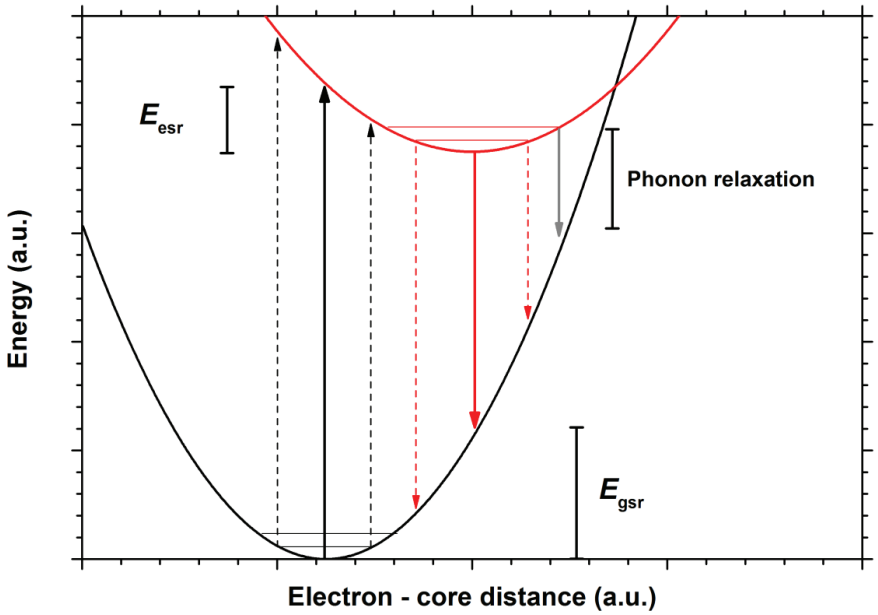

Figure 10: Configurational coordination diagram illustration showing the broadening of the absorption and emission peaks due to phonons and the Stoke shift coming from the parabolic shape of the energy curves. Phonon energies are represented by the horizontal lines near the bottom of the parabolas. E_{esr} and E_{gsr} is the excited state relaxation and ground state relaxation, respectively. The grey arrow illustrates phonon emission becoming dominant over photon emission.

The Laporte and spin selection rules the symmetry and strength of the crystal field, and the configurational coordination diagram goes a long way in explaining the optical absorption and emission properties of transition metal compounds and solutions. They also go a long way in explaining the optical properties of the lanthanides as well. The major difference between the d shell and f shell is that the f shell is shielded by filled s and p shells which have larger radii than the f orbitals. This reduces possibility of the surrounding atoms to push on the orbitals. The crystal field will have a much smaller effect on the energy of the orbitals, and all the excited states would lie directly above the ground state in a configurational coordination diagram. This is why lanthanide emissions are much less quenched by phonons, have almost no Stokes shift and show very narrow peaks. In addition, since all orbitals have the same energy, moving an electron between two orbitals requires almost no energy. In order

to have a higher energy state, two or more unpaired electrons must be paired. Thus, "all" transitions are both Laporte and spin forbidden. Thus the lanthanides often show very high emission yields as there is little phonon quenching and they show very long lifetimes since all the transitions are highly forbidden. A slight distortion of the symmetry of an f orbital will cause a slight lifting of the Laporte selection rule, and this can cause large difference in transition rate between this and other f orbitals. Thus, the lanthanides will have almost exactly the same energy position of the absorption and emission peaks in different compounds, but the transition rates can be different as the Laporte rule is very slightly lifted for some transitions depending on the symmetry crystal field.

For heavy elements like the lanthanides, we also have to consider spin-orbit coupling which is negligible for the early transition metals. This is a splitting of the energy levels caused by the interaction between the electrons spin and the magnetic field generated by the electron orbiting the atom. This causes a splitting of the energy levels of the lanthanides that are of the same magnitude as the splitting for the transition metals caused by the crystal field.

2.5 Term symbols and the Dieke diagram

Optical emission is the change from one excited state to a lower energy state (often the ground state). For the lanthanides, there are quite a few possible ways to distribute N_e electrons in the 7 f-orbitals. The total number of possible states is defined by eq. 2.2, where $l = 3$[*]. For Eu^{3+} which have $N_e = 6$ f-electrons, there are $N_{states} = 3003$ states spanning the entire range from VUV to NIR [51].

$$N_{\text{states}} = \frac{(2(2l+1))!}{N_e!\,(2(2l+1)-N_e)!} = \frac{14!}{N_e!\,(14-N_e)!} \qquad \textbf{(2.2)}$$

Many of these states are degenerate, meaning that they have the same energy. These states are grouped into one *level*. For example, one of the emission lines in the red luminescence spectrum of Eu^{3+} is written $^5D_0 \rightarrow {}^7F_2$.

[*] l = 0, 1, 2 and 3 is the s, p, d and f-shell. So all the states in the f-shell of the lanthanides have l = 3.

This means that the transition is between one of the *states* in the $^5D_0$ *level* and one of the *states* in the $^7F_2$ *level*. It is useful to have an understanding of what these term symbols mean so that they don't become just an abstract identification tag. The term symbol is define as $^{2S+1}L_J$, where S is the total spin quantum number, L the total orbital momentum quantum number* and J the total angular momentum quantum number. The *term* ^5D consists of all the *levels* ^5D_J which have a total spin S = 2† so that 2S + 1 = 5, and a total orbital momentum L = 2 which is written D in spectroscopic terms. For transition metals this would be enough, but the spin-orbit coupling further splits these levels for the heavier elements, thus we add the J term. The total angular momentum J can have the values J = L + S, L + S - 1 … |L – S| which in this case gives the 5 *levels* $^5D_{0–4}$. Each *level* contains 2J + 1 *states* which have the same total spin, total orbital momentum and total angular momentum and thus also have the same energy. The *level* $^5D_0$ thus consists of 1 *state*, $^5D_1$ consists of 3 *states* and so forth. When the absorbing or emitting atom is put into a crystal, these degenerate *states* are split by the crystal field, depending on the neighboring atoms and symmetry of which they surround it. As discussed earlier, this splitting is small for the shielded f shell compared to the splitting between the levels. These splittings are shown for NIR levels of Er^{3+} in Figure 11, showing that the *term* ^4I splits into several ^4I_J *levels* which consist of several states each. Thus, even though optical absorption and emission is the transition between *states*, we usually only specify the *level* they belong to.

* … written in spectroscopic terms. L = 0, 1, 2, 3, 4 etc. are written S, P, D, F, G and then continues alphabetically.

† i.e. 4 unpaired electrons, each having ½ spin each.

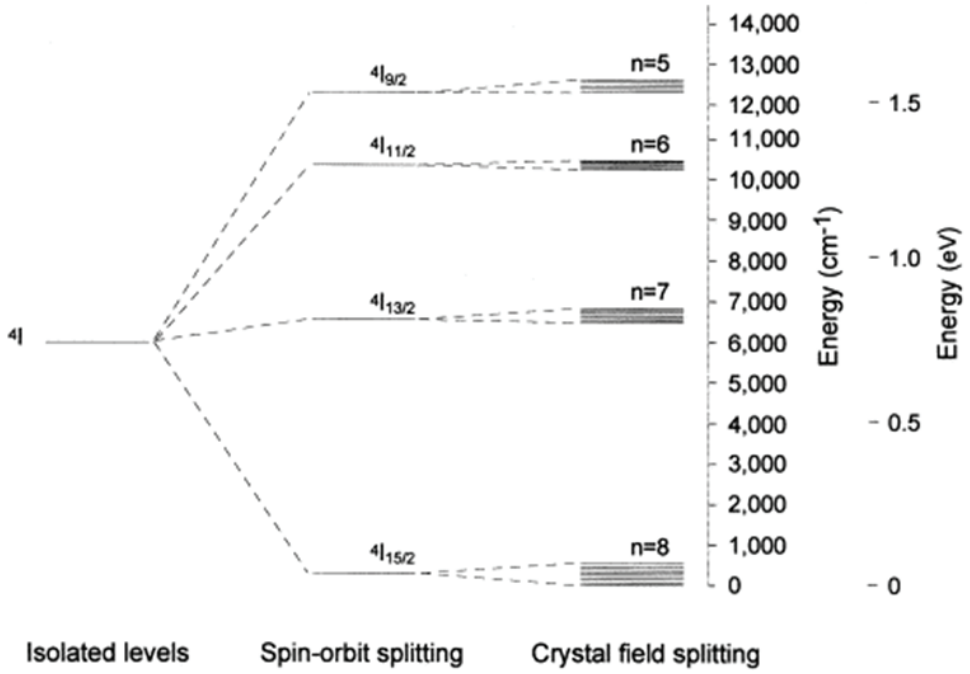

Figure 11: Energy level splitting in Er^{3+} caused by spin-orbit coupling and crystal field interactions, showing the *term* ^4I, the *levels* $^4I_{9/2}$ etc. and the individual *states* the levels are split into by the crystal field. The term n in this diagram denotes how many non-degenerate states the crystal field lead to in a certain silicate. Adapted and modified from [52].

These levels are the same, regardless of the surroundings of the atom. The only variation between different compounds containing the same lanthanide ion is very small splitting of each level caused by the crystal field. The major difference is usually how the crystal field affects the transition probabilities between the states, which can be substantial. Thus, as all the levels have the same energy, it is possible to form a diagram showing all the levels for all the trivalent lanthanide ions for all compounds under normal conditions. This is often called the Dieke diagram, after G. H. Dieke [53].

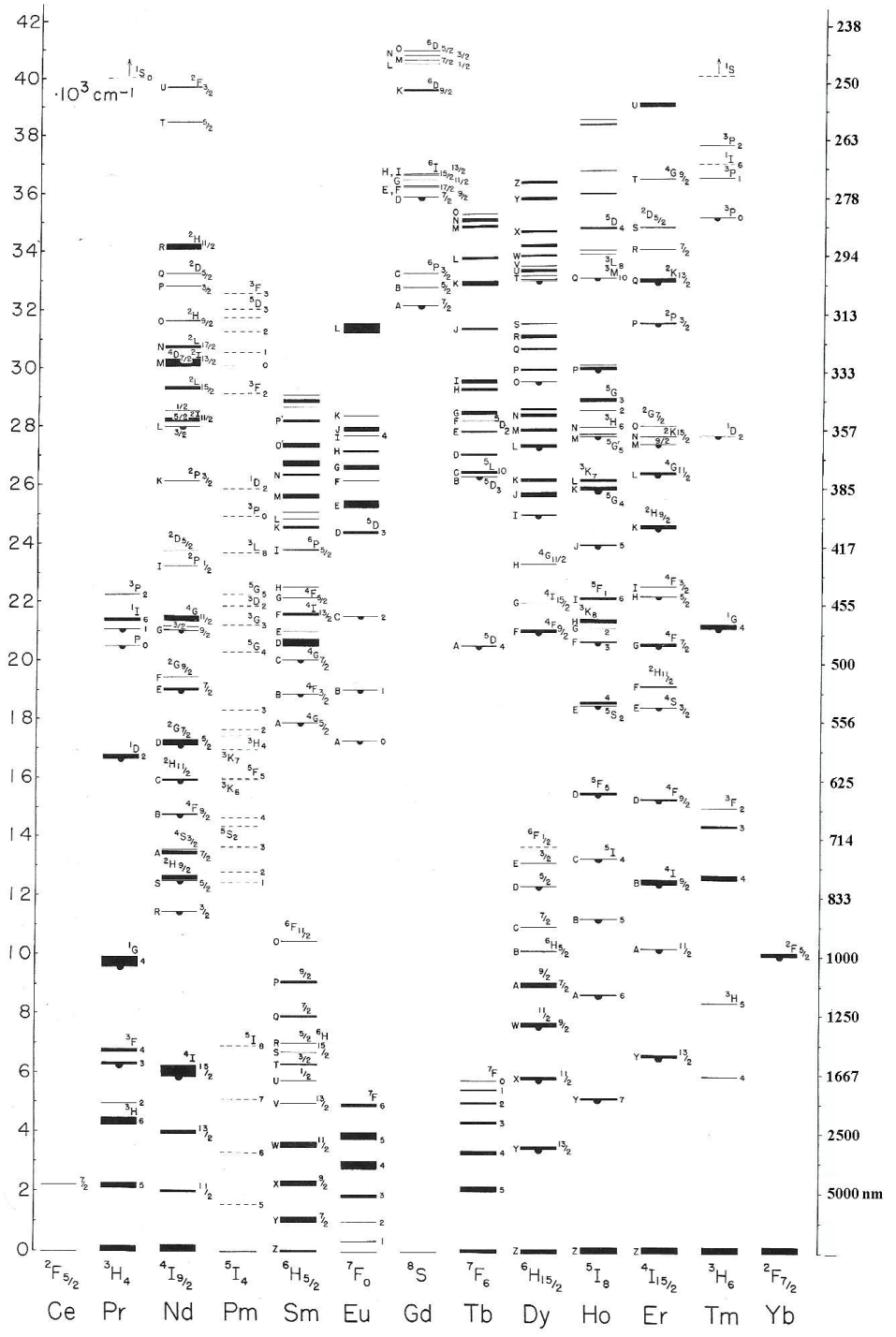

Figure 12: The Dieke diagram, modified to include wavelength units on the y-axis [53].

These splitting, the shielding of the f shell, term symbols, selection rules, and the differences between electric dipole (ED), magnetic dipole (MD), and electric quadropole (EQ) transitions regarding transition probabilities and symmetries are also explained Bünzli and Eliseeva [54][*].

2.6 Trivalent europium (Eu^{3+})

The emission spectrum from Eu^{3+} is of particular interest, not only because it is an important red phosphor, but because of the (often) relative simplicity of the spectrum. The emission stems from transitions between the $^5D_J \rightarrow {}^7F_J$ levels. The simplicity stems from the fast non-radiant $^5D_{J>0} \rightarrow {}^5D_0$ transitions and the fact that the $^5D_0$ level only contain a single state. Except in the cases where $^5D_1 \rightarrow {}^7F_J$ transitions occur in addition to the $^5D_0 \rightarrow {}^7F_J$ transitions, this means that when a splitting is observed in the different transitions, this originates only from the crystal field splitting of the ^7F_J levels. This in turn means that it is possible so learn something about the local symmetry by how the different emission peaks are split, as shown in Figure 14. Each emission line can only be split into as many lines as there are states in the ^7F_J level, thus the maximum splitting is 1, 3, 5 for the $^7F_0$, $^7F_1$, $^7F_2$ levels etc. Which level is split and into how many lines depend on the symmetry around the ion. Some examples of different splitting and transition probabilities are shown in Figure 13.

[*] I must admit that I didn't understand everything in this article when I first read it, but now that I have worked with the subject for some time I feel that it is a helpful reference when I need to re-read something.

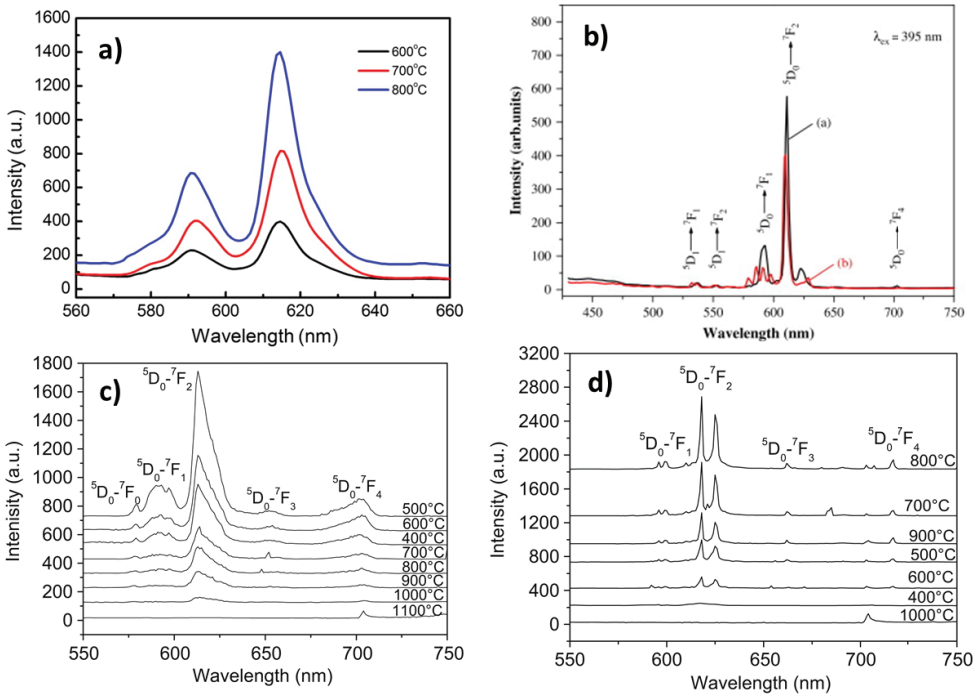

Figure 13: Luminescence spectra showing how different site symmetries of Eu^{3+} affect the $^5D_0 \rightarrow {}^7F_J$ emission. a) $CaZrO_3:Eu^{3+}$ at different annealing temperatures [55], b) $YNbTiO_6:Eu^{3+}$ (black) and commercial $Y_2O_3:Eu^{3+}$ (red) [56], c) solgel $TiSiO_4:Eu^{3+}$ [57], d) solgel $TiO_2:Eu^{3+}$ [57].

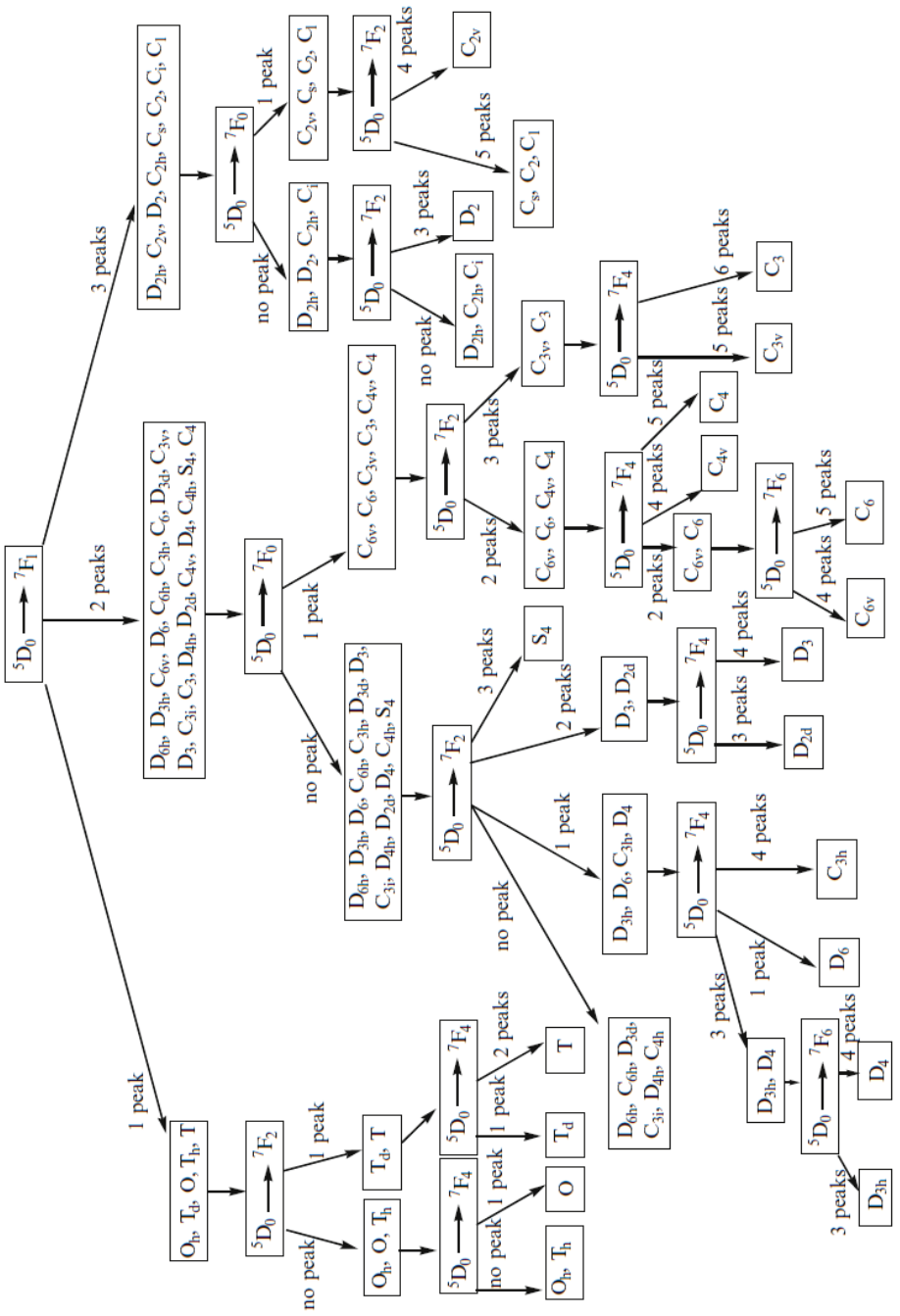

Figure 14: Site symmetry map from the emission spectrum of Eu^{3+} ions. Reprinted from [58].

Although Eu^{3+} is being used as a site symmetry probe in the literature, the emission spectra can be more complicated than it seems, and several misconception exists in the literature [51]. For example, some emission lines may be present even if they are parity forbidden as transition may be allowed through other mechanisms than electric dipole. In some systems, and often depending on the excitation wavelength, $^5D_1 \rightarrow {}^7F_J$ emissions may overlap with the normal $^5D_0 \rightarrow {}^7F_J$ spectrum. One should therefore be careful not to overinterpret these spectra.

2.7 Down conversion and energy transfer

Down conversion is any process where one high energy photon is absorbed and more-than-one photon is emitted. The energy range that is usually used for down conversion is the conversion of UV or VUV into visible or NIR photons*. The most common strategy to do this is to have one high energy level and one energy level at exactly half the energy. Both of these levels could be on the same atom and/or on different atoms or molecules. This way, several relaxation pathways exists from the high energy excited state which could give rise to more-than-one emission. This is illustrated in Figure 15. In practice, this is most often attempted with the f-f transitions of Ln^{3+} doped materials.

* Some X-ray and γ-ray detectors also work by converting one photon into hundreds or thousands of visible photons which are then detected by a photodiode or camera. Down conversion usually excludes these types of phosphors as the energy range and application is vastly different.

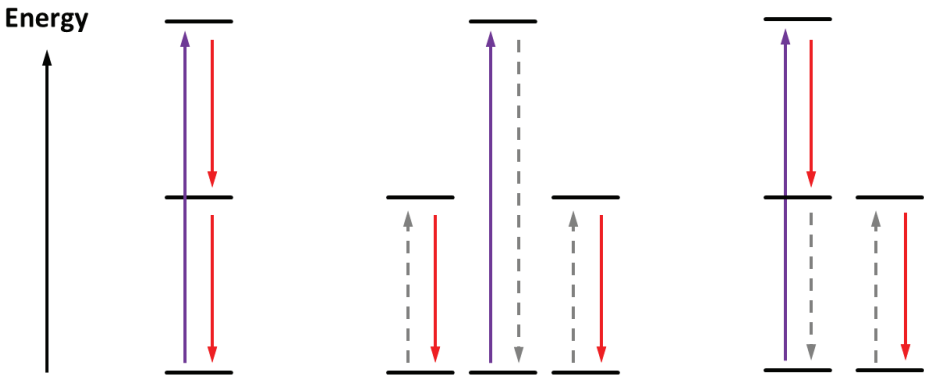

Figure 15: Illustration of three possible down conversion mechanisms. Left, stepwise emission from a single atom. Middle, two simultaneous Förster energy transfers and subsequent emissions via two neighboring atoms. Right, emission followed by Förster energy transfer and a second emission.

One of the main research interests for down conversion have been for fluorescent lighting. A lot of energy is wasted by down shifting the 254 nm mercury emission in these lights. These photons could potentially be down converted into 550 nm or longer photons, which would reduce energy loss and heating in the phosphor material. In addition, mercury free fluorescent lights are being developed using Xe as UV source, emitting 147 and 172 nm photons in low and high Xe pressure respectively. The higher energy of these photons increases the energy losses in the phosphor, increasing the need for down conversion for these lamps to be competitive. There are several papers that report very high quantum efficiencies for VUV to visible light down conversion. Two examples are 190 % for 202 nm → red light in $LiGdF_4:Eu^{3+}$ [59] and 194 % for the same process in $BaF_2:Eu^{3+},Gd^{3+}$ [60]. The down conversion mechanism is illustrated in Figure 16. In this system, the excitation of the ^6P_J level of Gd^{3+} will result in the full $^5D_J \rightarrow {}^7F_J$ emissions of Eu^{3+}. Excitation of the ^6G_J level of Gd^{3+} on the other hand will give a higher amount of $^5D_0 \rightarrow {}^7F_J$ emissions, if the suggested down conversion mechanism is efficient.

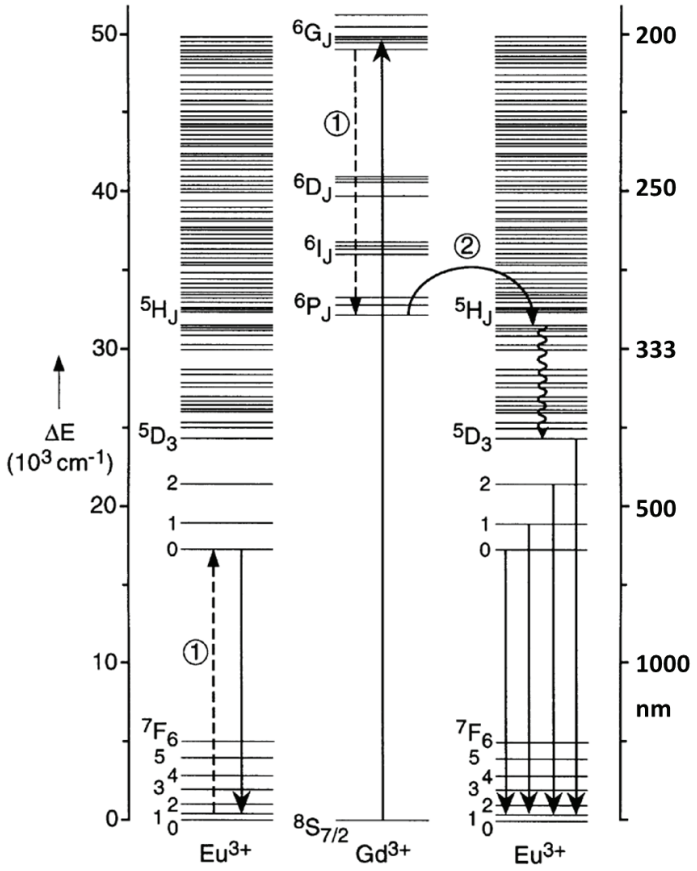

Figure 16: Down conversion mechanism in the Gd^{3+}/Eu^{3+} pair. Step 1 is a Förster energy transfer from Gd^{3+} to Eu^{3+} causing only $^5D_0 \rightarrow {}^7F_J$ emission. Step 2 is another Förster energy transfer, but this may cause a full range of $^5D_J \rightarrow {}^7F_J$ emissions. Reprinted and modified to include wavelength on the y-axis from Wegh *et al*. [59].

During the last two decades, a rapidly increasing interest has been given to down conversion related to solar cells as well. For silicon solar cells, the emission from Yb^{3+} is ideal and thus much interest has been given to $Ln^{3+} – Yb^{3+}$ based down conversion materials where Ln^{3+} = Ce^{3+}, Pr^{3+}, Tb^{3+}, Tm^{3+}. The d-f transition of Ce^{3+} and f-f transitions of the others could enable the down conversion of < 500 nm photons. There are today quite a few papers reporting down conversion with Yb^{3+} emission that have a quantum efficiency above 150 %. A good summary of the field of down conversion of both VUV → Vis and UV/blue → 980 nm up until 2008 is given by Zhang *et al*. [28], including tables

of all the reported materials and efficiencies. Unfortunately, it is sometimes difficult to understand what exactly is meant when such efficiencies are reported. The absolute quantum efficiency, as in photons in vs photons out, is usually not measured. The efficiencies are more often based on how the ratios between emission lines depend on the excitation wavelength (as in Figure 16), or by lifetime measurement. These types of measurements do indeed say something about the efficiency of the energy transfer processes. The absolute quantum efficiency however may be lower* as quenching by phonon relaxation or by defects are usually ignored when emission efficiency of the emitting states are assumed to be 100 %†.

One thing that is sure however, is that down conversion for solar cells will most likely involve the energy transfer between lanthanides and/or the energy transfer between a UV-absorbing host or molecule and a lanthanide. Seemingly, this is most often due to a Förster type energy transfer, which is the simultaneous relaxation of one atom and excitation of one or more other atoms. This transfer rate is inversely proportional to the sixth power of the distance between the two atoms. As a general rule, this type of energy transfer can be efficient up to around 1 nm distances. As the atoms come closer and closer, the transfer rate should increase drastically. In addition, it is proportional to the spectral overlap integral, which is the overlap between the emission spectrum of the excited atom and absorption spectrum of the receiving atom. Thus, in order to get efficient energy transfer, it is crucial to have the right atoms in the right atomic arrangement.

There is another type of energy transfer often mentioned regarding phosphors as well, called the Dexter energy transfer. This is also sometimes called the short range or collisional energy transfer. In this transfer, the excited electron of the donor jumps over into an excited state of the acceptor while a ground state electron of the acceptor jumps over to the ground state of the donor. In addition to the spectral overlap, the Dexter energy transfer requires

* Personally, I find it puzzling that there exist green Tb^{3+}-based phosphors with close to 100 % efficiency and apparently $Tb^{3+} \rightarrow Yb^{3+}$ energy transfer with more than 180 % efficiency, but nobody has yet demonstrated a silicon solar cell with > 100 % quantum efficiency in the UV range.

† I.e. once the energy is transferred, all excited states are assumed to produce a photon with 100 % efficiency.

the overlap of the wave functions of the orbitals that the electrons occupy. As atoms have to be very close for this to happen[*], this energy transfer can often occur mainly during the collision between two molecules. Hence the name collisional energy transfer. As the f orbitals are shielded by the larger s and p shell, the overlap between the wave function of the f orbital on one lanthanide and an f orbital on a second lanthanide with an anion between them should be insignificant. Thus, any non-radiative energy transfer between two lanthanides is likely to be exclusively of the Förster type.

[*] A covalent bond requires the overlap of the orbital wavefunctions, so this bond distance can be used as a rule of thumb of the short distance required.

Chapter 3 – Atomic layer deposition

3.1 The basics

Atomic layer deposition* (ALD) is a quite unique thin film deposition technique. It is similar to chemical vapor deposition (CVD), but differs in how the precursors are introduced into the reaction chamber. In CVD the precursors are introduced simultaneously and careful control of the substrate temperature, gas flows and the chamber pressure allows continuous film growth on the substrates while preventing the precursors from reacting with each other directly in the gas phase. In ALD, the precursors are introduced sequentially with an inert gas purge between each precursor pulse. This sequential pulsing separated by purging enables the use of extremely reactive precursors which can react rapidly at low and even room temperature. Thus, ALD is a relative low temperature deposition technique with deposition temperatures usually in the 200 – 400 °C range. This also enables deposition on substrates that cannot withstand the higher temperatures of CVD, like plastic and even textiles.

When a precursor is pulsed into the chamber, it will after a short time saturate all surfaces in the chamber. The precursor should not decompose or react with its own surface species, and thus a single layer is produced which renders the surfaces inert to further adsorption of that precursor. The leftover precursor in the gas phase is flushed away by the inert purge. When the second precursor is pulsed into the chamber, it will react with the surface species from the first precursor and saturate the surfaces with its own surface species. This is then repeated hundreds or thousands of times to obtain the wanted film thickness. The process is illustrated in Figure 17 with the precursor pair trimethylaluminium (TMA) and water, which reacts explosively when mixed to together.

* Also called atomic layer epitaxy (ALE) and atomic layer chemical vapor deposition (ALCVD).

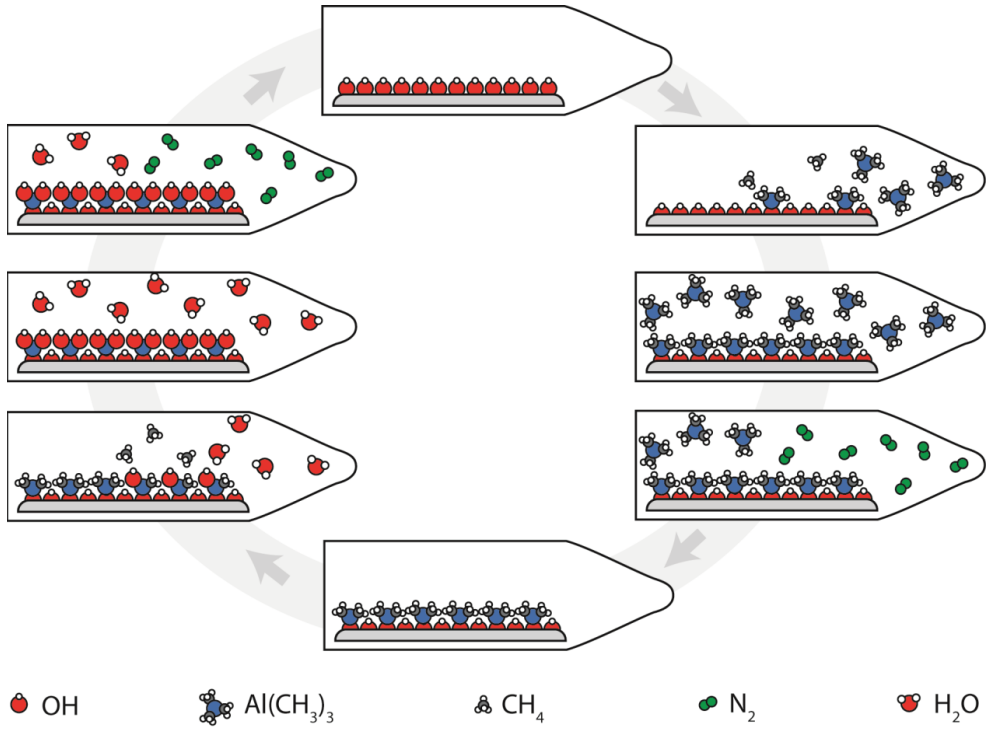

Figure 17: Illustration of the cyclical nature of ALD growth. Reprinted with permission from Ingrid Vee [61].

The strengths of ALD are the combination of excellent 3D coverage, pin-hole free films and the layer-by-layer growth which enables complex multilayer structures and doping profiles. In addition to academic research, ALD has also found industrial application. A review from 2009 by Ritala *et al*. [62] describes the benefits and limitations of ALD in an industrial perspective and gives examples of commercial use of ALD in among other microelectronics and optics.

3.2 Single and multicomponent oxides

Binary oxides like Al_2O_3 and TiO_2 are usually quite simple to deposit by ALD. It is usually simply a matter of choosing a sufficiently reactive precursor pair which is compatible with the substrates and temperatures used. At least, this is the case for cations which have one strongly preferred oxidation state. If the cation

(or anion) can have several different oxidation states, like manganese for example, more care have to be put into choosing the right precursors which favors the wanted compound. Also, if the cation (or anion) is very mobile in the deposited material, like lithium often is, this also complicates the growth compared to the "ideal" ALD in Figure 17. Today, most binary oxides have been successfully deposited by ALD.

Depositing multicomponent oxides by ALD is in theory simple by alternating between the two binary oxide cycles. For example, if one wants to deposit $Al_xTi_yO_z$ with varying stoichiometries, one could alternative between TMA/H_2O and $TiCl_4$/H_2O cycles in different ratios. In practice it is at least a bit more complicated than that. Even if the two binary oxide cycles are completely compatible, i.e. they don't cause any unwanted reactions, a binary oxide often grows a bit differently on itself than on a surface coated by another oxide. In addition, one has to be careful when including a cation (or anion) that can have multiple oxidation states. For example, if one of the binary oxides is MnO, then the cycle for the second binary oxide should not include a very strong oxidant as that is likely to oxidize the MnO to a higher valent oxide.

The field of ALD has been growing rapidly in the past few decades and the number of different materials which have been deposited by ALD increases every year. These include binary and multicomponent oxides, elemental metals, nitrides, sulfides, phosphates, carbonates and almost any class of materials is represented. Thus, in order to keep an overview over the development, review articles describing the recent and past progresses are published from time to time. The latest review while writing this thesis is by Miikkulainen *et al*. [63].

3.3 Light emitting materials by ALD

The early developments of the ALD field were partly driven by the development of electroluminescent (EL) displays [64]. One of the first classes of materials deposited was transition metal and lanthanide doped ZnS and alkaline earth sulfides. A complete overview of the different types of precursors which have been employed can be found in ref. [63], thus only the materials and dopants* will be repeated here. Dopants in ZnS includes ZnS:Mn^{2+} [65-67],

* The charge of the dopant is only given where the charge is specified in the literature.

ZnS:(Ce,Tb,Eu,Tm) [68]. ALD have also been used to fabricated inverse opal structures of ZnS:Mn^{2+} [69, 70] and TiO_2/ZnS:Mn^{2+} [71]. Doped alkaline earth sulfides includes BaS:Ce [72], SrS:Cu [73, 74], SrS:Ce [75, 76], Sr:(Cu,Pb,Ce,Mn,Eu) and BaS:(Ce,Mn,Eu) [77], CaS:Pb^{2+} [78], (Ca,Sr,Ba)S:Tb^{3+} [79]. This research topic has also been extended to include other II-IV materials as in $SrS_{1-x}Se_x$:Ce and $ZnS_{1-x}Se_x$:Mn [80], self-organized quantum dots of $Cd_{1-x}Mn_xTe$ [81] and CdSe:Mn [82], CdSe/ZnSe and CdTe/ZnTe quantum well structures [83]. Luminescent InGaAs has been grown both as films [84] and self-organized quantum dots [85, 86]. Lately, the ALD of Er^{3+} containing oxide films have been studied as optical gain media in Er_2O_3 [87], Y_2O_3:Er^{3+} [88, 89] and Y_2O_3:Er^{3+},Yb^{3+} [90] in addition to up conversion in Al_2O_3:Er^{3+} [91].

3.4 ALD and non-ALD lanthanide titanate thin films

Both lanthanide oxides and titanium oxides grown by ALD have been reported in literature. For the lanthanides, the $Ln(thd)_3/O_3$ pair (Hthd = 2,2,6,6-tetramethyl-3,5-heptanedione) has been utilized the most while for TiO_2 the $TiCl_4/H_2O$ precursor pair is one of the most well known ALD systems, as seen in the ALD review mentioned earlier [63]. Although both the deposition of LnO_x and TiO_2 is well known and both materials are technologically important materials, to my knowledge there are only two reports combining these two materials in an ALD film. This lanthanum titanate by the $La(thd)_3/O_3$ and $TiCl_4/H_2O$ process [92], and erbium titanate by the tris(methylcyclopentadienyl)erbium/O_3 and tetrakis(diethylamino)titanium/O_3 processes [93]. These materials were developed for lithium battery and high-k dielectric materials, respectively.

Several lanthanide titanate films for luminescence purposes have been deposited by other techniques though. In particular the sol-gel technique is popular which have been used to deposit single and codoped titanates: Eu [94-100], Er [101, 102], Eu and Er [103], Y and Er [104], Tb and Gd [105], Y, Er, Tm and Yb [106], Nd, Sm, Eu, Tb, Er, Tm and Yb [107]. Additional film deposition techniques include titanates of Eu by xerogel [108] and evaporation induced self-assembly [109], Tm and Yb by MOCVD [110], Sm and Ey nanoparticle film [111], Sm by spray pyrolysis [112] and Eu, Tm and Yb by PLD [113]. These films include amorphous, anatase, rutile and cubic pyrochlore $Y_2Ti_2O_7$ phases. A

common denominator for all of these depositions is that the distribution of cations will be random. I have not been able to find much work that focuses on the distribution of lanthanides aside from varying the concentrations.

3.5 Post deposition rapid thermal annealing (RTA)

ALD often results in amorphous films, especially if the film is a multicomponent material. For most materials, this is a metastable state which is only hindered from crystallizing by the low mobility of the atoms to reposition themselves. Heating such amorphous films usually results in crystallization at some higher temperature, depending of the type of material. Annealing such samples enables the investigation of how materials properties relate to the crystal structure, or lack thereof.

Rapid thermal annealing (RTA), or rapid thermal processing (RTP) as it is also called, is a technique to rapidly heat a sample to high temperatures for a short time by illuminating the sample chamber with high power lamps. This is usually done in vacuum. Thus, the energy is transferred by radiation in contrast to convection in a regular oven. The implication is that the heating of the sample depends on the reflectivity and absorptivity of the sample. This makes exact temperature control difficult as different types of samples will absorb different amounts of energy, but the reproducibility should be high. All annealed samples in this work have been transparent thin films on silicon, where the silicon is responsible for most of the absorption of energy.

Chapter 4 – Characterization techniques

Several characterization techniques have been used in this work. All of these techniques are however quite standard in material research and are well described in the literature. This chapter will thus only give a brief description of the different techniques and instruments used.

4.1 Spectroscopic ellipsometry

Spectroscopic ellipsometry is an optical reflection technique which utilizes the difference in reflectivity of s- and p-polarized light at an interface to investigate optical properties like $n(\lambda)$ and $k(\lambda)$ and the thickness of the sample. The properties of the sample are found by modeling the measurement data. The complexity of this technique depends strongly on the optical complexity of the sample. In this work, two ellipsometers with different spectrum ranges was used and the modeling was done with the CompleteEASE software, all from J. A. Woollam Co.

For standard thickness measurements, an alpha-SE spectroscopic ellipsometer (390 – 900 nm) instrument was used. All samples are fully transparent in this range. A Cauchy function was thus sufficient to model the film material. To investigate the UV absorption properties of titania containing samples, a VASE variable angle spectroscopic ellipsometer (260 – 1100 nm)[*] instrument was used. To model these materials in the UV range, a Tauc-Lorentz oscillator was used.

[*] The full range of this instrument was 250 – 2500 nm, but only the smaller 260 – 1100 nm range was used for practical reasons.

4.2 Optical spectroscopy (UV-Vis-NIR)

Optical transmission measurements were conducted on films deposited on soda lime glass in the range 180 – 3300 nm with a Shimadzu UV-3600 instrument. Three detectors were used that cover different ranges: photomultiplier tube (180 – 900 nm), InGaAs photodiode (900 – 1700 nm) and PbS photodiode (1700 – 3300 nm). All samples were highly transparent, apart from the strong UV absorption of the titania containing films. The weak f-f transitions were only detectable for some of the lanthanide oxides, while this absorption was too weak to detect for all titania containing films.

4.3 Photoluminescence (PL)

Photoluminescence (PL) was conducted on films deposited on Si(100). The excitation source was a HeCd 325 nm laser while an USB4000 spectrometer from OceanOptics was used as a detector. The laser is s-polarized with respect to the sample surface and at an incident angle of 23° while the detector was positioned normal to the sample surface. Samples were measured in batches to reduce the effects of fluctuations in the laser intensity etc. between the samples. When a new batch of samples was measured, several samples from the previous batch were also measured to be able to compare samples between batches.

4.4 X-ray diffraction (XRD)

All samples were characterized by X-ray diffraction (XRD) in θ-2θ reflection geometry to investigate the crystallinity of the deposited material. A Bruker D8 Discover diffractometer with Cu $K_{\alpha 1}$ and a Ge(111) monochromator and a LynxEye detector was used for this. XRD in this geometry can only detect crystal planes parallel to the sample surface. In thin film depositions one sometimes obtains partly or fully oriented growth. Compared to XRD of powder samples where crystallites are randomly oriented, this can result in fewer diffraction peaks than expected and changes in the relative peak intensities. In particular when very few peaks are observed and several phases are possible, determining the crystalline phase(s) can be difficult for thin films.

4.5 X-ray reflectivity (XRR)

The multilayer structures presented in article III were characterized by X-ray reflectivity (XRR) to investigate the layer structure, or lack thereof. A PANalytical Empyrean diffractometer with Cu radiation[*], parallel beam mirror, 0.27° parallel plate collimator and a proportional Xe detector was used for this. This technique relies on the reflectivity of X-rays from materials at low incident angles. Most materials have $n(\lambda) < 1$ in the X-ray range resulting in total "internal" reflection[†] from the sample when the incident angle is below the critical angle. Thus, at angles slightly higher than the critical angle the X-ray reflectivity is at its maximum and an interference pattern is (often) observed between the beams reflected from the air/sample and the sample/substrate interfaces. From these patterns several sample properties can be modeled: the thickness is related to the wavelength of the interference pattern, the roughness is related to the dampening of the amplitude of the interference pattern and the density of the film material is related to the critical angle. Each interface in multilayer structures can also contribute to the interference pattern, which is why XRR is quite good at characterizing thin multilayer structures.

4.6 X-ray fluorescence (XRF)

In X-ray fluorescence, a core electron is excited by the incident X-ray beam. When the electron relaxes back down to a lower energy orbital, X-rays are emitted. These energies are specific to the orbital energies involved in the transition which are unique to each element. The fluorescence spectrum is thus unique to each element. XRF is therefore an ideal non-destructive tool to determine the elemental composition of the sample. Concentrations down to 1 – 10 ppm can be measured for solid samples, while for thin films the detection limit is in practice closer to 1 % due to the relatively small amount of sample material. The X-ray fluorescence was measured on a Philips PW2400 instrument and analyzed using the UniQuant software.

[*] No monochromator to maximize intensity.

[†] For visible light, all materials have $n(\lambda) > 1$ so that total internal reflection happens on the material side of the air/material interface. For X-rays it is opposite as air has a higher $n(\lambda)$ than materials.

4.7 Atomic force microscopy (AFM)

Atomic force microscopy (AFM) can be used to characterize the surface of a sample by scanning the surface in a xy pattern with a very thin needle tip and measuring the force between the tip and the surface. For amorphous materials, the useful characteristic is the surface roughness, while for crystalline samples the crystallite sizes, shapes and distribution can be visualized. In this work, a Park XE70 atomic force microscope in tapping mode was used for the lanthanide oxide films while contact mode was used for the titanate containing films. The sample area was usually a $5 \times 5\ \mu m^2$ area.

4.8 Field emission scanning electron microscopy (FESEM)

In this work, AFM has been the main characterization tool for surface topography. One sample however, ALD grown PrO_x, proved difficult to characterize with AFM, thus field emission scanning microscopy (FESEM) was employed for this sample. FESEM is very similar to a "normal" SEM with the exception that the cathode has been replaced with a field emission cathode which provides a narrower probing beam. In practice, a FESEM gives higher spatial resolution than a regular SEM and have lower requirements for the conductivity of the sample as the lower electron flux in the narrower beam causes less charging of the sample surface. The FESEM characterization on this sample was done for us by an engineer at the FEI Corporation on Nova™ NanoSEM 650.

Chapter 5 – Results and discussion

The goal of this work has been to develop thin film synthesis routes of luminescent lanthanide based oxide materials by ALD, with the long term aim of obtaining down conversion. One of the strengths of ALD is the relative ease of depositing multicomponent materials, as long as the deposition of the binary compounds is known. Thus, this work has been a stepwise process. First, obtaining deposition parameters for simple lanthanide oxides, secondly to combine this with a UV absorbing oxide to form a down shifting material, thirdly to investigate the possibility to make sub-nanometer layer structures, and lastly to make sub-nanometer layer structures of the UV absorbing oxide and multiple lanthanides in the hopes of obtaining a down conversion material.

5.1 Deposition of lanthanide oxides (paper I)

The deposition of all the lanthanides by $Ln(thd)_3$ and ozone at 300 °C have been reported in the literature earlier, with the exception of Pr and only to a very limited extent Tb. This paper fills in the lacking data in the whole 200 – 400 °C range and reports on the deposition of Pr and Tb oxides. All the deposited lanthanide oxides followed the same trends, with the exception of Pr and Tb. The trends were: growth rate increasing with temperature, amorphous at low deposition temperatures and crystalline above a certain temperature (250 – 300 °C depending on the lanthanide) and an optical absorption due to f-f transitions which changed as the crystallinity changed. The optical absorption due to f-f transitions depend on the local symmetry around the lanthanide ion, and thus also the crystallinity or lack thereof. As exemplified by the Nd depositions in Figure 18, there is a clear correlation between the crystal phase and peak positions in the optical absorption spectra of the film material. The

XRD reflections due to cubic Ln_2O_3 are marked with (hkl) and a reflection due to the hexagonal phase is marked “Hex.”.

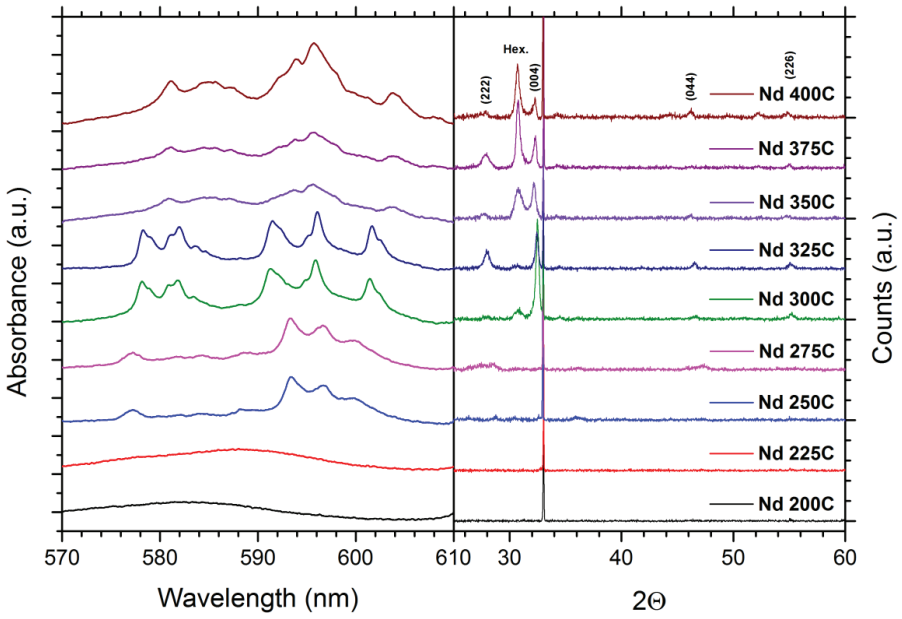

Figure 18: Optical absorbance (left) and XRD data for the Nd_2O_3 depositions deposited at 200 – 400 °C (right). A clear correlation is seen between the crystallinity and peak positions in the optical absorbance with four distinct temperature ranges: ≤ 225 °C are too thin to properly distinguish any absorption peaks, 250 – 275 °C amorphous, 300 – 325 °C cubic, ≥ 350 °C cubic and hexagonal.

One interesting result here is the different growth mechanisms for $Pr(thd)_3$ and $Tb(thd)_3$ which resulted in thickness gradients, and for $Pr(thd)_3$ also a very structured surface coming from the higher degree of crystallinity and preferred orientation of these samples, Figure 19. This is likely due to these two lanthanides preference for a mixed $Ln^{3+/4+}$ state in oxide materials. The same would probably be the case for $Ce(thd)_3$ and ozone, but previous experience with these precursors at our group show that it deposits as Ce^{4+} as CeO_2 which doesn’t have any f electrons. Thus this was not included in this work. It is unfortunate that deposition of Pr and Tb oxides resulted in mixed oxidation states as Pr^{3+}/Yb^{3+} and Tb^{3+}/Yb^{3+} is two of the lanthanide pairs most often showing possibility for down conversion in the literature. One conclusion

of this paper is that if pure Pr^{3+} and Tb^{3+} containing materials are required, the thd and ozone process is likely not suitable.

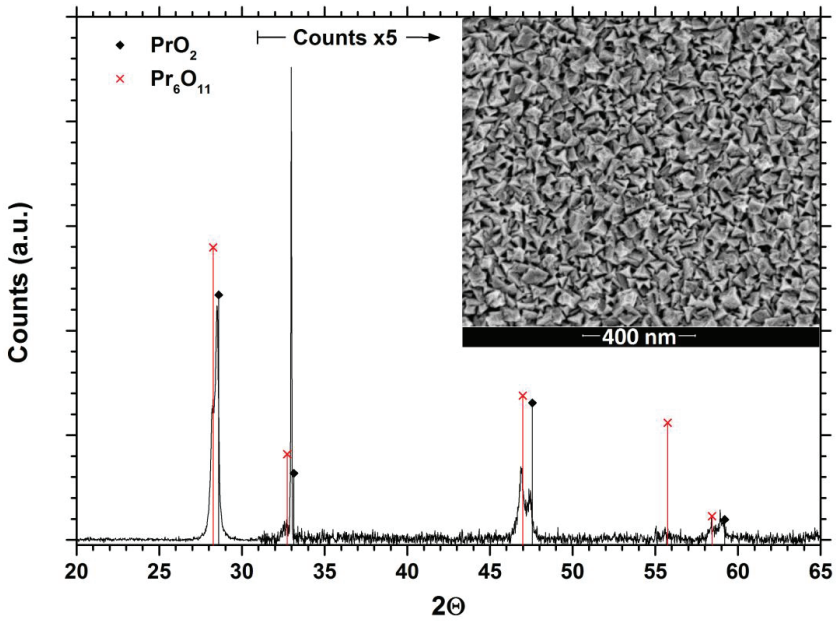

Figure 19: XRD data and FESEM image of a $Pr(thd)_3$ / ozone deposition at 300 °C. The sharp reflection at 2θ = 33° is from the Si substrate.

5.2 Deposition of europium titanate (paper II)

In this work, TiO_2 was chosen as the UV absorbing oxide due to its deposition by $TiCl_4$ and H_2O being well known in the literature. The three most used lanthanides in luminescent oxides are Ce^{3+}, Eu^{3+} and Tb^{3+}. As paper I and earlier experience showed, cerium and terbium doesn't deposit as pure Ln^{3+} by the $Ln(thd)_3$ / ozone precursor pairs, thus europium was chosen. The films compositions were varied by alternating between different numbers of $Eu(thd)_3$ / ozone and $TiCl_4$ / H_2O cycles. The Eu – Ti oxide did indeed luminesce, which neither TiO_2 nor Eu_2O_3 did under the same 325 nm excitation, proving the energy transfer between the TiO_2 and Eu^{3+} ions. The titanium heavy samples (< 30 % Eu_2O_3 cycles) deposited as a mixture of amorphous $Eu_xTi_yO_z$ and Eu^{3+} doped anatase, while only amorphous $Eu_xTi_yO_z$ was obtained for 30 % and higher Eu_2O_3 cycles. For approximately 80 nm thick films, the highest

luminescence was obtained for 50 % Eu_2O_3 cycles. The luminescence spectrum of the amorphous phase and the total luminescence intensity is plotted in Figure 20. The luminescence spectrum of Eu^{3+}-doped anatase is shown in the bottom spectrum in Figure 23. The luminescence spectrum of the deposition containing between 10 and 20 % Eu_2O_3 cycles were superpositions of these two spectra.

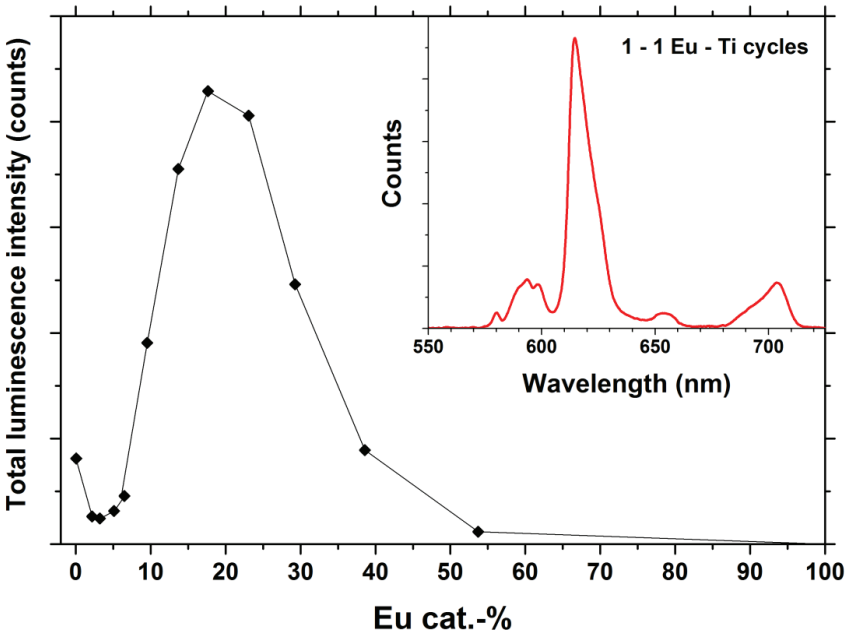

Figure 20: Luminescence spectrum of a sample of depositions of 50 % cycle ratio Eu_2O_3 (inset), and total luminescence intensity of all samples with varying cycle ratios. The most luminescent sample is the 50 % cycle ratio sample, containing 17.7 cat.-% Eu.

I did find two results obtained in this work surprising however. First, the amorphous phase did show much stronger luminescence than the crystalline $Eu_2Ti_2O_7$ phase obtained by annealing. The luminescence intensity of the samples decreased with increasing annealing temperature and was practically zero when annealed at 700 °C. These depositions showed no crystalline phases by XRD, but samples annealed at 1000 °C contained crystalline $Eu_2Ti_2O_7$ and rutile. Literature and textbooks often give the impression that large single crystals always give better luminescence, but this is in fact not always true. Berdowski *et al*. found that crystalline $Eu_2Ti_2O_7$ show no luminescence at room

temperature [114], while Blasse *et al*. found that luminescence could be observed from Eu^{3+}-doped $Gd_2Ti_2O_7$ with the same structure [115]. Thus, as also argued by these authors, it seems like there are a strong concentration quenching effect in this crystal system. Berdowski argues that this is due to the excitation transferring between Eu^{3+}-ions until it reaches a quenching site, like an impurity atom. Figure 21 shows $n(\lambda)$ and $k(\lambda)$ for the annealed samples. Annealing up to and including 600 °C did not cause any change in $n(\lambda)$ and $k(\lambda)$, while higher annealing temperatures caused an increase in $k(\lambda)$. This supports the idea that small crystallites, or clusters, starts to form in the amorphous material when annealing at 600 – 700 °C.

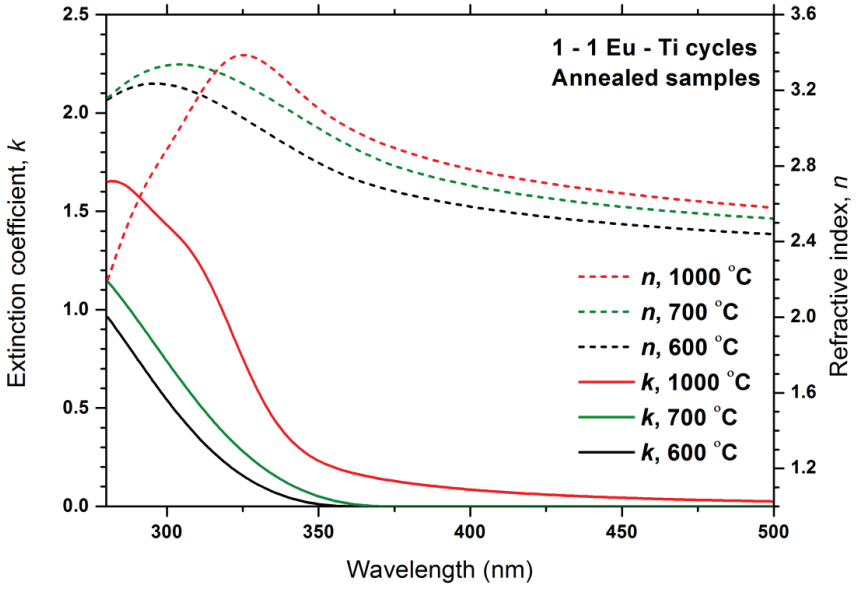

Figure 21: Extinction coefficient and refractive index of annealed samples of depositions of alternating Eu_2O_3 and TiO_2 cycles (1-to-1 cycle ratio). As-deposited samples and samples annealed up to and including 600 °C have identical $k(\lambda)$ and $n(\lambda)$. This data is not included in paper II.

Secondly, I did expect concentration quenching for the europium heavy samples. This also did not seem to be the case for the amorphous samples, but rather the decrease in luminescence is likely simply due to the low content of Ti^{4+} in these samples. This is in agreement with the findings of Ovenstone *et al.* [116, 117]. The pure $Eu_xTi_yO_z$ samples also showed a very smooth surface (RMS

roughness < 0.3 nm), showing that this system has potentially good properties as an optical film material. However, the luminescence of these samples was quenched by annealing, due to the formation of $Eu_2Ti_2O_7$. Eu^{3+}-doped nanocrystals of monoclinic $La_2Ti_2O_7$ [118] and cubic Y–Ti–O [100] on the other hand are luminescent. Thus, it might be possible to avoid the quenching $Eu_2Ti_2O_7$ phase by alloying with La^{3+} or Y^{3+} which are larger and smaller in size compared to Eu^{3+}.

5.3 Deposition of multilayer structures (paper III)

The purpose of this paper was to investigate if the layer-by-layer growth of ALD would enable a controlled sub-nanometer layer structure which would later be needed for the controlled mixing of the Ti^{4+} and different Ln^{3+} ions. In order to investigate this, the relative ratio of Eu_2O_3 and TiO_2 cycles and total number of cycles was kept constant and supercycles of N Eu_2O_3 + N TiO_2 cycles were deposited while varying N from 1 – 50. The PL spectra shape was found to be independent of N while the total PL intensity was almost constant for N = 1 – 10 and decreased for higher N, as seen in the inset in Figure 22. Identical PL spectra indicate that the luminescent Eu^{3+} is in the same local symmetry in all the samples. There were no practical difference between the samples $n(\lambda)$ and $k(\lambda)$, and no crystal phases were detected by XRD. Thus, the major difference between the samples should be the distances and mixing of the Eu^{3+} and Ti^{4+} cations.

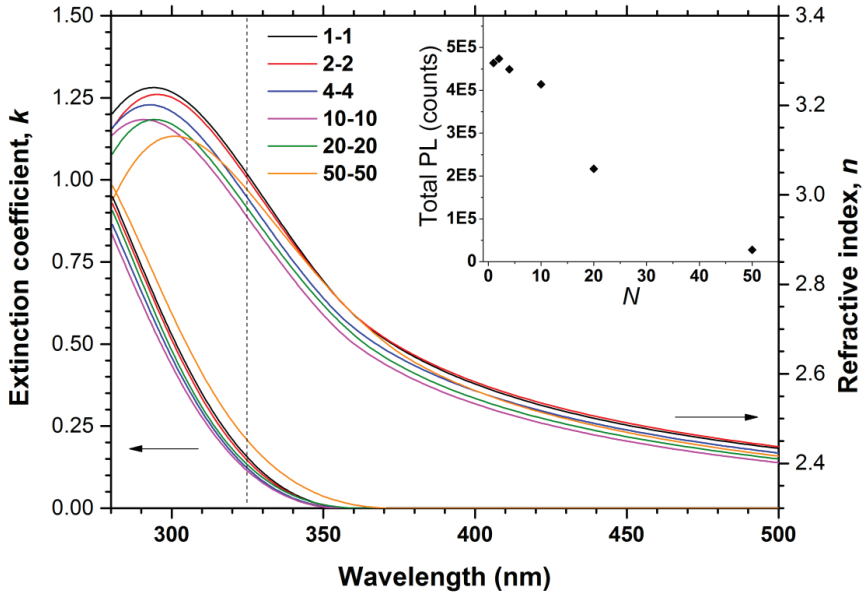

Figure 22: Extinction coefficient and refractive index of the layered samples, showing that *n*(λ) and *k*(λ) is fairly independent of *N*. The stapled line at 325 nm shows the excitation wavelength. The inset shows how the total luminescence intensity varies with the layer thickness *N*.

XRR showed that the N = 10 sample did indeed have a distinct layer structure. The 10 Eu_2O_3 + 10 TiO_2 superlayer was found to be 0.75 nm thick, while it was not possible to determine the individual Eu_2O_3 and TiO_2 layers. However, this implies that at least one of the layers is less than 0.4 nm thick. This is approximately the same as one Eu – Eu distance in crystalline Eu_2O_3. In conclusion, this means that by ALD and the $Ln(thd)_3$ / ozone + $TiCl_4$ / H_2O precursor pairs, it is possible to make sub-nanometer layer structures, giving a very unique control of the spatial distribution of the different cations.

5.4 Comments on paper II and III

During the work on paper II and III, four different PL spectra were encountered. Four illustrative examples are shown in Figure 23. All the $Eu_xTi_yO_z$ with 30 % or more Eu_2O_3 cycles, layered structures and 50 % Eu_2O_3 cycles deposited at different temperatures showed spectrum corresponding to "$Eu_xTi_yO_z$" in the

figure as deposited. This spectrum is typical of amorphous Eu-Ti-O materials found in literature. The sample with the lowest Eu content showed a typical Eu^{3+}-doped anatase spectrum. The samples ranging from 10 – 20 % Eu_2O_3 cycles showed a superposition of these two spectra, with a ratio depending on the Eu content. The two spectra illustrated by "800 °C anneal" and "900 °C anneal, 50N" are from for now unknown phases. The "900 °C anneal, 50N" spectrum was only seen for the *N* = 50 layered structure annealed at 900 °C, while the other was seen for all the layered samples and 50 % Eu_2O_3 cycles samples deposited at different temperatures when annealed at 800 °C. No crystal phases could be identified by XRD for these samples, but the differences in the spectra indicate that the local symmetry around the luminescent Eu^{3+} ions is different.

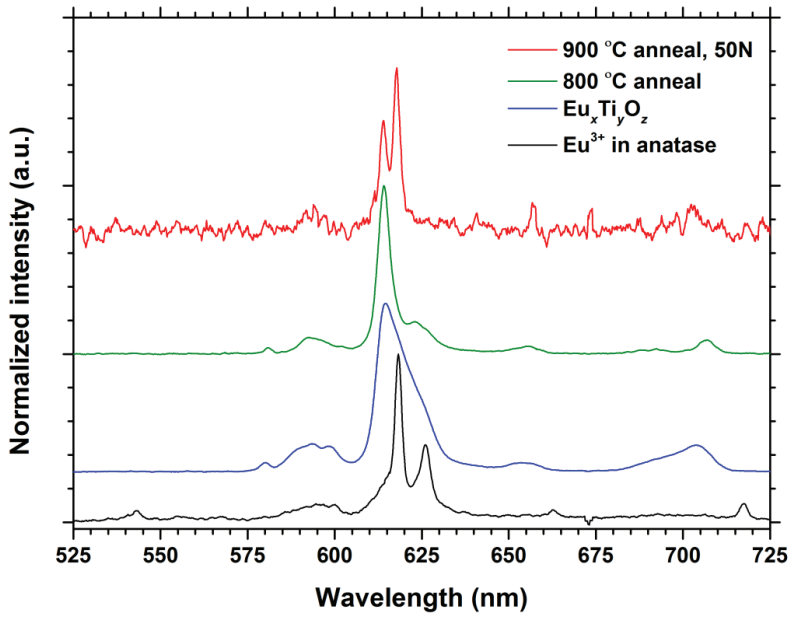

Figure 23: The four different types of Eu^{3+} luminescence spectra obtained in paper II and III. Comparing these with literature spectra, the as deposited bottom curve matches well with Eu^{3+}-doped anatase and the $Eu_xTi_yO_z$ matches with amorphous europium titanium oxides. The other two types of spectra are only seen upon annealing. This data is combined from paper II and III.

Amorphous materials are metastable, and will crystallize if given the chance (by annealing for example). Which crystal phase precipitates depends

on several factors however, like composition, kinetics, temperature, annealing conditions like time and ramp rate etc. A certain phase may be the thermodynamically stable phase at a certain temperature, but other phases may have already precipitated by the time the sample reaches this temperature and kinetics may prevent a phase change between those phases. Thus, it is not trivial to estimate a priori what phases are likely to be present, even when the composition and annealing conditions are known.

Some aspects are clear however. Any annealing at 500 °C or higher will cause precipitation in the amorphous phase. At 700 °C, there seems to be no amorphous material left as no luminescence is detected, except for the layered $N \geq 20$ samples. For these samples, there is an increase of the luminescence for annealing up to and including 650 °C. This could possibly be due to the separated Eu^{3+} and Ti^{4+} cations mixing, but without forming any crystallites as the PL spectra are still identical for annealing up to and including 700 °C. At 800 °C annealing, the sample deposited at 375 °C and the layered film with $2 \leq N$ show the third type of spectrum named “800 °C anneal” in Figure 23. The Eu content is slightly higher for these samples than the 1N sample and samples deposited at 300 and 225 °C, which showed no luminescence when annealed at 800 °C. The samples which showed the third type of spectrum decreased in luminescence intensity when annealed at the 800 °C for longer times. Thus it can seem that whatever the phase which is formed at 800 °C is, it is a metastable one which given enough time or thermal energy will turn into another non-luminescent phase. At 900 °C annealing, no sample show any detectable luminescence apart from the 50N sample which show the distinct fourth type of spectrum named “900 °C anneal, 50N”. No samples show any detectable luminescence when annealed at 1000 °C.

There are obviously a lot of unexplained diffusion, atomic rearranging and crystallization happening in this system upon annealing. Unfortunately, with the tools (and knowledge) available to me at this point, it has not been possible to elucidate this any further. In fact a lot of the discussion in the last paragraph could be claimed to be simple speculations until the possible crystal structures or local symmetries could be experimentally determined.

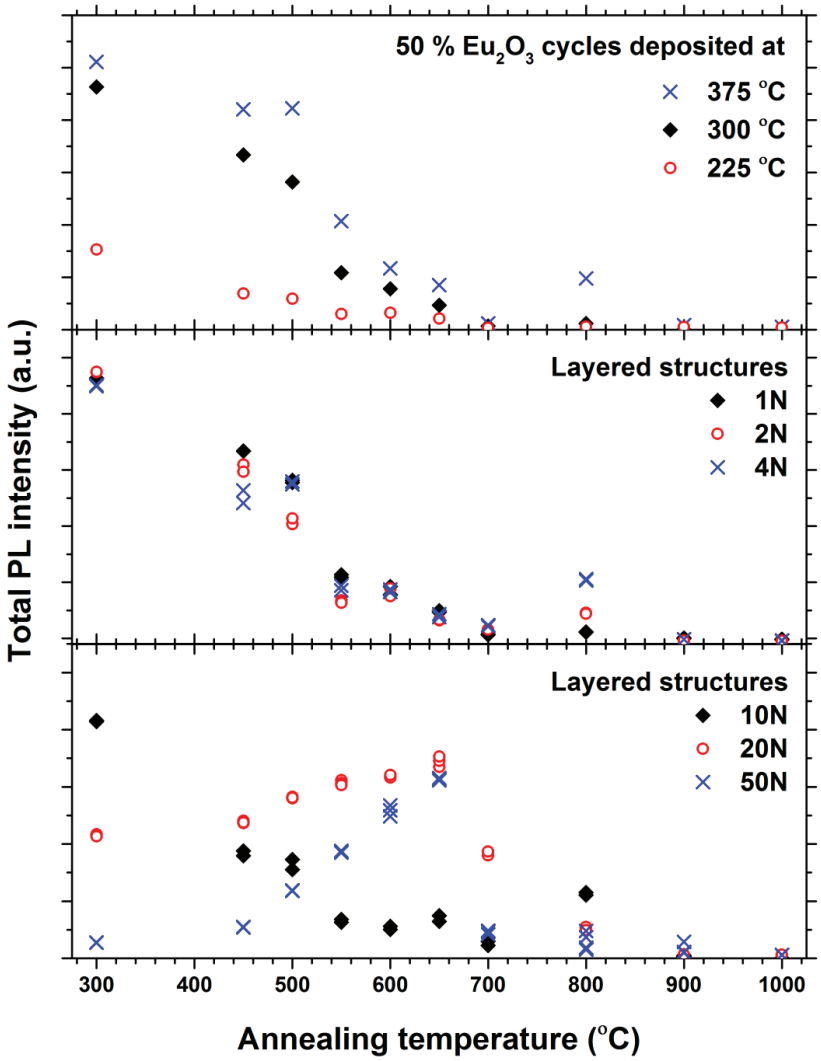

Figure 24: Total PL intensity (525 – 725 nm range) for annealed samples.

5.5 Deposition of lanthanide titanates (paper IV)

This paper attempts to use the results from the previous 3 papers to obtain a down conversion material, using Yb^{3+} for 980 nm emission. The literature show that Ce^{3+}, Pr^{3+}, Tb^{3+} and Tm^{3+} combined with Yb^{3+} potentially can lead to down conversion. As neither of the lanthanides absorbs much UV light, except Ce^{3+}

which could not be deposited by our precursor pair, TiO_2 was still needed. The goal was then to achieve efficient energy transfer from TiO_2 to Ln^{3+} and from Ln^{3+} to 2 Yb^{3+} which then emits one 980 nm photon each.

The first part of paper IV investigates the energy transfer between TiO_2 and Ln^{3+}. Similar samples as the $Eu_xTi_yO_z$ in paper II were made by alternating between Ln_2O_3 and TiO_2 cycles. All $Ln_xTi_yO_z$ samples showed some luminescence. The $La_xTi_yO_z$ sample showed a weak and broad emission, similar to the broad luminescence from pure TiO_2 samples. This broad emission was completely absent in all other $Ln_xTi_yO_z$ samples which indicates that energy transfer from TiO_2 to Ln^{3+} dominates over this "intrinsic" emission observed from the $La_xTi_yO_z$. Even though the energy transfer from the TiO_2 to the Ln^{3+} apparently was efficient, all the Ln^{3+} emissions were about two orders of magnitude weaker than the Eu^{3+} emission. Annealing the samples decreased the luminescence intensity for all samples, including the broad emission from $La_xTi_yO_z$, apart from the Nd^{3+} and Sm^{3+} samples. For these two samples the PL spectrum shape changed and the intensity increased for annealing temperatures up to 800 °C, but decreased to zero for 1000 °C. This is like due to the larger size of these lanthanides compared to the others, causing the crystallites formed during the annealing to adopt a different type of structure.

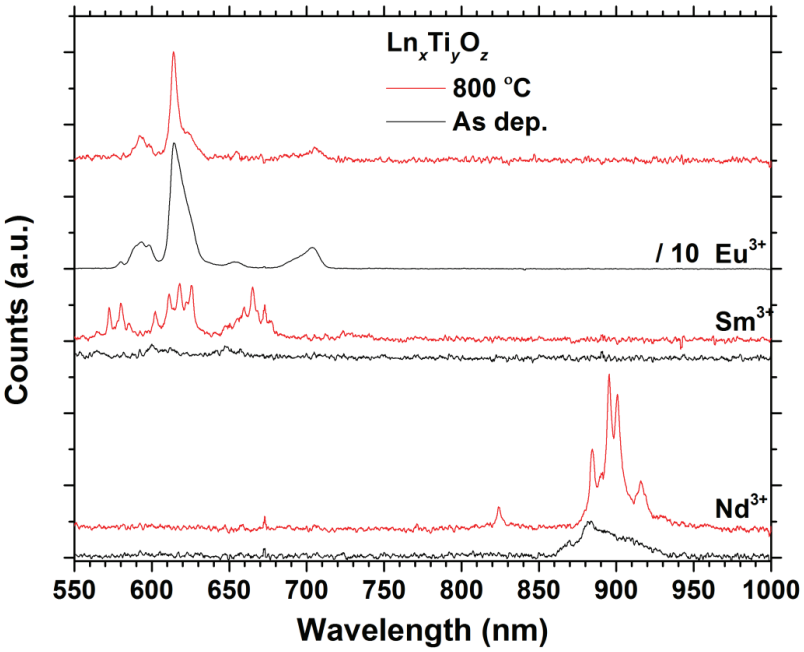

Figure 25: Luminescence spectra of the $Ln_xTi_yO_z$ samples containing Nd, Sm and Eu. The spectra of the samples annealed at 800 °C are obviously from Ln^{3+} in a different local symmetry than in the as deposited samples.

The second part of paper IV regards the deposition of $Ti^{4+}/Ln^{3+}/Yb^{3+}$ samples in the hopes of obtaining down conversion. The layer structure was obtained by repeating supercycles of Yb_2O_3 / Ln_2O_3 / Yb_2O_3 / 3 TiO_2 cycles. This structure should give the optimal situation for down conversion due to the very close proximity of the Ti^{4+} and Ln^{3+}, and that all Ln^{3+} should have plenty of Yb^{3+} next neighbors. The Yb^{3+} emission from the $(La,Yb)_xTi_yO_z$ sample was taken as a base value, and any increase or decrease in this emissions intensity in the other $(Ln,Yb)_xTi_yO_z$ samples would indicate an energy transfer between Ln^{3+} and Yb^{3+}. An increase would not by itself prove that down conversion was achieved though. Unfortunately, the Yb^{3+} emission was completely quenched by the addition of Pr, Sm, Dy, Ho and Tm and remained unaffected by Nd, Eu, Tb and Er. For Er^{3+}, there seems to be a modest increase in the Yb^{3+} emission, but the Er^{3+} has a similar emission in the same range. The 1550 nm emission of Er^{3+} was visible, indicating that the apparent increase in Yb^{3+} emission is simply a superposition of the two spectra. Annealing only decreased the total emission

intensity for all samples, including the Nd^{3+} and Sm^{3+} containing samples. Thus, we were unfortunately not able to obtain down conversion this time.

On the bright side though, the 1200 nm emission of Ho^{3+} was much stronger in the $(Ho,Yb)_xTi_yO_z$ sample than in the $Ho_xTi_yO_z$ sample, indicating that Yb^{3+} is an efficient sensitizer for Ho^{3+} in this system.

Chapter 6 – Concluding remarks

Down conversion was not observed in this work. Nevertheless, some progress has been made that indicate that ALD is still a potentially fruitful approach for thin film down conversion. The results of paper III show that it is possible to control the separation and mixing of different cations down to the unit cell level. This is not generally true for all precursor systems, but having this type of control is "simply" a matter choosing the right precursors. A distinct separation of the layers of less than 0.4 nm is well below the range that the Förster energy transfer is efficient, which is in general assumed to be 1 – 5 nm. Thus, controlling the local concentration of different cations and which types of atoms that are in "talking distance" to each other should indeed be possible with ALD, at least in the growth direction. Some control of the separation is also possible in the growth plane by controlling the size of precursors or the number and distribution of active surface sites.

Perhaps the largest obstacle to achieve down conversion during this work was the inability to produce pure Ce^{3+}, Pr^{3+} and Tb^{3+} from $Ln(thd)_3$ and ozone. These three lanthanides along with Tm^{3+} are the most used partner to Yb^{3+} in Ln^{3+}/Yb^{3+} down conversion pairs. Thus, as long as the strategy for obtaining down conversion is through Ln^{3+}/Yb^{3+} pairs, other precursors have to be used. As the three problematic lanthanides easily forms Ln^{4+}, the oxygen source have to be very weakly oxidizing. Otherwise, and Ln^{3+} that is formed will immediately be oxidized to Ln^{4+}. This requires the lanthanide precursor to be much more reactive that the $Ln(thd)_3$ compounds are. In the review of the ALD field by Miikkulainen *et al*. [63], no reports of pure Ce^{3+}, Pr^{3+} or Tb^{3+} oxides exists as of 2013. Another alternative would be the *ex-situ* reduction of the material. Attemps at reducing a TbO_x film by hydrogen at high temperatures have been made by Joachim Svendsen at our group, which was unsuccessful in

obtaining pure Tb^{3+}. I therefore believe that *in-situ* growth of pure Ln^{3+} is a more fruitful approach.

A second issue in this work is that Tm^{3+} quenches the Yb^{3+} emission in the deposited films. The same is also true for Pr^{3+}, which most likely contained a mixture of Pr^{3+} and Pr^{4+}. Thus, perhaps the $Ln_xTi_yO_z$ system is not well suited for this type of light conversion. Titanates are in fact not very common hosts for phosphor materials. Looking at the phosphor literature, oxysulfide, sulfides, fluorides, vanadates and yttrium aluminium garnets are more common materials. It might be useful to attempt to deposit these known materials to have a better starting point to work with. In particular sulfides, fluorides and other halogens could be beneficial as they are less oxidizing that oxygen so it is unlikely that Ln^{4+} would exist in these hosts.

While searching the literature for works on down conversion, a host of different materials, crystal structures, micro structures and ion pairs is being investigated throughout the world. Two additional things also become apparent. One, although there are no lack of creativity in the many different types of synthesis techniques reported, they all have in common that the distribution of the different lanthanide ions is random. The distribution of the lanthanides can only be influenced by controlling the overall and relative concentrations. And two, no material that efficiently down converts sunlight exists as of today. Thus, I do believe that ALD can provide a unique arena to tackle the problem of developing down conversion materials for solar cells by introducing a unique control of the atomic neighborhood. By choosing better host materials more suited for luminescent materials than titanates, and choosing a precursor system that prevents the formation of Ln^{4+}, ALD should be a well suited synthesis routes for down conversion materials. Hopefully, the future will tell…

References

1. IPCC, *Climate Change 2013: The Physical Science Basis.* IPCC Fifth Assessment Report, 2013.
2. IPCC, *Climate Change 2013: The Physical Science Basis - Summary for Policymakers.* IPCC Fifth Assessment Report, 2013.
3. B. Metz, O.R.D., P.R. Bosch, R. Dave, L.A. Meyer, *Climate Change 2007: Mitigation of Climate Change.* IPCC Fourth Assessment Report, 2007.
4. Jacobson, M.Z. and M.A. Delucchi, *Providing all global energy with wind, water, and solar power, Part I: Technologies, energy resources, quantities and areas of infrastructure, and materials.* Energy Policy, 2011. **39**(3): p. 1154-1169.
5. Delucchi, M.A. and M.Z. Jacobson, *Providing all global energy with wind, water, and solar power, Part II: Reliability, system and transmission costs, and policies.* Energy Policy, 2011. **39**(3): p. 1170-1190.
6. Mathys, N.A., *Feasibility Study for "Revealing the Scale of Subsidies to Fossil Fuels".* The Global Subsidies Initiative, 2007.
7. Lucy Kitson, P.W., Tom Moerenhout, *Subsidies and External Costs in Electric Power Generation: A comparative review of estimates.* International Institute for Sustainable Development, 2011.
8. Bazilian, M., et al., *Re-considering the economics of photovoltaic power.* Renewable Energy, 2013. **53**(0): p. 329-338.
9. REN21, *Renewables 2012 Global Status Report.* 2012.
10. Solangi, K.H., et al., *A review on global solar energy policy.* Renewable and Sustainable Energy Reviews, 2011. **15**(4): p. 2149-2163.
11. Moosavian, S.M., et al., *Energy policy to promote photovoltaic generation.* Renewable and Sustainable Energy Reviews, 2013. **25**(0): p. 44-58.
12. IPCC, *Renewable Energy Sources and Climate Change Mitigation.* Special Report of the Intergovernmental Panel on Climate Change, 2012.
13. Tsoutsos, T., N. Frantzeskaki, and V. Gekas, *Environmental impacts from the solar energy technologies.* Energy Policy, 2005. **33**(3): p. 289-296.
14. Jäger-Waldau, A., *Research, Solar Cell Production and Market Implementation of Photovoltaics.* PV Status Report 2012, 2012.
15. Würfel, P., *Physics of Solar Cells: From Principles to New Concepts*. 2005: WILEY-VCH Verlag GmbH & Co.

16. Green, M.A., *Solar Cells: Operating Principles, Technology, and System Applications*. 1992: University of New South Wales.
17. Nelson, J., *The Physics of Solar Cells*. 2003: Imperial College Press.
18. Shockley, W. and H.J. Queisser, *Detailed Balance Limit of Efficiency of p-n Junction Solar Cells.* Journal of Applied Physics, 1961. **32**(3): p. 510-519.
19. Nick84. *http://commons.wikimedia.org/wiki/File:Solar_spectrum_en.svg*. Wikimedia Commons 2013, Accessed 25/10/2013.
20. NREL. *http://www.nrel.gov/ncpv/images/efficiency_chart.jpg*. Accessed 26/03/2014.
21. Green, M.A., *The path to 25% silicon solar cell efficiency: History of silicon cell evolution.* Progress in Photovoltaics: Research and Applications, 2009. **17**(3): p. 183-189.
22. Panasonic. *Panasonic HIT® Solar Cell Achieves World's Highest Energy Conversion Efficiency of 25.6% at Research Level*. Accessed 02/05/2014; Available from: http://panasonic.co.jp/corp/news/official.data/data.dir/2014/04/en140410-4/en140410-4.html.
23. SunPower. *http://us.sunpowercorp.com/homes/products-services/solar-panels/x-series/*. Accessed 25/10/2013.
24. Klampaftis, E., et al., *Enhancing the performance of solar cells via luminescent down-shifting of the incident spectrum: A review.* Solar Energy Materials and Solar Cells, 2009. **93**(8): p. 1182-1194.
25. Chen, J.Y., et al., *Efficiency improvement of Si solar cells using metal-enhanced nanophosphor fluorescence.* Solar Energy Materials and Solar Cells, 2014. **120, Part A**(0): p. 168-174.
26. Trupke, T., M.A. Green, and P. Wurfel, *Improving solar cell efficiencies by down-conversion of high-energy photons.* Journal of Applied Physics, 2002. **92**(3): p. 1668-1674.
27. Richards, B.S., *Luminescent layers for enhanced silicon solar cell performance: Down-conversion.* Solar Energy Materials and Solar Cells, 2006. **90**(9): p. 1189-1207.
28. Zhang, Q.Y. and X.Y. Huang, *Recent progress in quantum cutting phosphors.* Progress in Materials Science, 2010. **55**(5): p. 353-427.
29. Trupke, T., M.A. Green, and P. Würfel, *Improving solar cell efficiencies by up-conversion of sub-band-gap light.* Journal of Applied Physics, 2002. **92**(7): p. 4117-4122.
30. Trupke, T., et al., *Efficiency enhancement of solar cells by luminescent up-conversion of sunlight.* Solar Energy Materials and Solar Cells, 2006. **90**(18-19): p. 3327-3338.

31. Shalav, A., B.S. Richards, and M.A. Green, *Luminescent layers for enhanced silicon solar cell performance: Up-conversion.* Solar Energy Materials and Solar Cells, 2007. **91**(9): p. 829-842.
32. Singh-Rachford, T.N. and F.N. Castellano, *Photon upconversion based on sensitized triplet–triplet annihilation.* Coordination Chemistry Reviews, 2010. **254**(21–22): p. 2560-2573.
33. Gibart, P., et al., *Below Band-Gap IR Response of Substrate-Free GaAs Solar Cells Using Two-Photon Up-Conversion.* Japanese Journal of Applied Physics, 1996. **35**(Part 1, No. 8): p. 4401.
34. Pan, A.C., C. del Cañizo, and A. Luque, *Characterization of up-converter layers on bifacial silicon solar cells.* Materials Science and Engineering: B, 2009. **159–160**(0): p. 212-215.
35. Richards, B.S. and A. Shalav, *Enhancing the Near-Infrared Spectral Response of Silicon Optoelectronic Devices via Up-Conversion.* Electron Devices, IEEE Transactions on, 2007. **54**(10): p. 2679-2684.
36. Cheng, Y.Y., et al., *Improving the light-harvesting of amorphous silicon solar cells with photochemical upconversion.* Energy & Environmental Science, 2012. **5**(5): p. 6953-6959.
37. Ende, B.M.v.d., L. Aarts, and A. Meijerink, *Lanthanide ions as spectral converters for solar cells*. 2009, Royal Society of Chemistry.
38. Marichy, C., M. Bechelany, and N. Pinna, *Atomic Layer Deposition of Nanostructured Materials for Energy and Environmental Applications.* Advanced Materials, 2012. **24**(8): p. 1017-1032.
39. Aarik, J., et al., *Morphology and structure of TiO2 thin films grown by atomic layer deposition.* Journal of Crystal Growth, 1995. **148**(3): p. 268-275.
40. Jakschik, S., et al., *Crystallization behavior of thin ALD-Al_2O_3 films.* Thin Solid Films, 2003. **425**(1–2): p. 216-220.
41. Schuisky, M., et al., *Atomic Layer Chemical Vapor Deposition of TiO_2 Low Temperature Epitaxy of Rutile and Anatase.* Journal of The Electrochemical Society, 2000. **147**(9): p. 3319-3325.
42. Wang, H., S. Xu, and R.G. Gordon, *Low Temperature Epitaxial Growth of High Permittivity Rutile TiO_2 on SnO_2.* Electrochemical and Solid-State Letters, 2010. **13**(9): p. G75-G78.
43. Gringer, P.R., *http://commons.wikimedia.org/wiki/File:EM_spectrumrevised.png*. Wikimedia Commons, 2013, Accessed 25/10/2013.
44. FDominec, *http://commons.wikimedia.org/wiki/File:Ruby_transmittance.svg*. Wikimedia Commons, 2008, Accessed 25/10/2013.

45. Lavinsky, R., http://commons.wikimedia.org/wiki/File:Corundum-215478.jpg. Wikimedia Commons, 2010, Accessed 25/10/2013.
46. D.328, http://commons.wikimedia.org/wiki/File:Artificial_ruby_hemisphere_under_a_monochromatic_light.jpg. Wikimedia Commons, 2011, Accessed 25/10/2013.
47. D.328, http://commons.wikimedia.org/wiki/File:Artificial_ruby_hemisphere_under_a_normal_light.jpg. Wikimedia Commons, 2011, Accessed 25/10/2013.
48. Jüstel, T., H. Nikol, and C. Ronda, *New Developments in the Field of Luminescent Materials for Lighting and Displays.* Angewandte Chemie International Edition, 1998. **37**(22): p. 3084-3103.
49. Fleischauer, P.D. and P. Fleischauer, *Photoluminescence of transition metal coordination compounds.* Chemical Reviews, 1970. **70**(2): p. 199-230.
50. Verstegen, J.M.P.J., *The Luminescence of Tb^{3+} in Borates of the Composition $X_2Z(BO_3)_2$ (X = Ba , Sr , Ca ; Z = Ca , Mg)* Journal of The Electrochemical Society, 1974. **121**(12): p. 1631-1633.
51. Tanner, P.A., *Some misconceptions concerning the electronic spectra of tri-positive europium and cerium.* Chemical Society Reviews, 2013. **42**(12): p. 5090-5101.
52. Kenyon, A.J., *Recent developments in rare-earth doped materials for optoelectronics.* Progress in Quantum Electronics, 2002. **26**(4–5): p. 225-284.
53. Dieke, G.H., H.M. Crosswhite, and H. Crosswhite, *Spectra and energy levels of rare earth ions in crystals*. 1968: Interscience Publishers.
54. Bünzli, J.-C. and S. Eliseeva, *Basics of Lanthanide Photophysics*, in *Lanthanide Luminescence*, P. Hänninen and H. Härmä, Editors. 2011, Springer Berlin Heidelberg. p. 1-45.
55. Du, Q., et al., *Combustion synthesis and photoluminescence properties of $CaZrO_3$: Eu^{3+} with highly enhanced brightness by Li^+ doping.* Journal of Luminescence, 2013. **137**(0): p. 83-87.
56. Ma, Q., et al., *Synthesis and optical properties of novel red phosphors $YNbTiO_6$:Eu^{3+} with highly enhanced brightness by Li^+ doping.* Solid State Sciences, 2009. **11**(6): p. 1124-1130.
57. Berkani, O., et al., *Effects of heat treatment and TiO_2 content on the optical properties of Eu^{3+} doped TiO_2–SiO_2 thin films.* Journal of Luminescence, 2012. **132**(11): p. 2979-2983.

58. Tanner, P., *Lanthanide Luminescence in Solids*, in *Lanthanide Luminescence*, P. Hänninen and H. Härmä, Editors. 2011, Springer Berlin Heidelberg. p. 183-233.
59. Wegh, R.T., et al., *Visible quantum cutting in Eu^{3+}-doped gadolinium fluorides via downconversion.* Journal of Luminescence, 1999. **82**(2): p. 93-104.
60. Liu, B., et al., *Visible quantum cutting in BaF_2:Gd,Eu via downconversion.* Journal of Luminescence, 2003. **101**(1-2): p. 155-159.
61. Vee, I., *Fluorholdige hybridmaterialer med atomlagsavsetting : Syntese og karakterisering.* Master thesis, University of Oslo, 2012.
62. Ritala, M. and J. Niinisto, *Industrial Applications of Atomic Layer Deposition.* ECS Transactions, 2009. **25**(8): p. 641-652.
63. Miikkulainen, V., et al., *Crystallinity of inorganic films grown by atomic layer deposition: Overview and general trends.* Journal of Applied Physics, 2013. **113**(2): p. 021301.
64. Mikko Ritala, M.L., *Atomic Layer Deposition*, in *Handbook of Thin Film Materials*, H.S. Nalwa, Editor. 2001, Academic Press. p. 103 - 159.
65. Ihanus, J., et al., *Aging of electroluminescent ZnS:Mn thin films deposited by atomic layer deposition processes.* Journal of Applied Physics, 2005. **98**(11): p. 113526.
66. N.A. Vlasenko, Y.F.K., Z.L. Denisova, Yu.V. Kopytko, L.I. Veligura, El. Soininen, R.O. Tцrnqvist and K.M. Vasama, *Aging of ZnS:Mn thin - film electroluminescent devices grown by two different atomic-layer epitaxial processes.* Semiconductor Physics, Quantum Electronics & Optoelectronics, 2001. **4**: p. 48-55.
67. Stuyven G., V.P., Neyts K., Hikavyy A., *Hybrid Electroluminescent Devices with Atomic Layer Deposited Thin Films on a Screen Printed Dielectric.* Japanese Journal of Applied Physics, 2002. **41**(Part 1, No. 9): p. 5702-5705.
68. Tammenmaa, M., et al., *Zinc sulphide thin films doped with rare earth ions.* Journal of the Less Common Metals, 1986. **126**(0): p. 209-214.
69. King, J.S., et al., *High-filling-fraction inverted ZnS opals fabricated by atomic layer deposition.* Applied Physics Letters, 2003. **83**(13): p. 2566-2568.
70. King, J.S., et al., *ZnS-based photonic crystal phosphors fabricated using atomic layer deposition.* physica status solidi (b), 2004. **241**(3): p. 763-766.
71. King, J.S., E. Graugnard, and C.J. Summers, *Photoluminescence modification by high-order photonic bands in TiO_2/ZnS:Mn multilayer inverse opals.* Applied Physics Letters, 2006. **88**(8): p. 081109-3.

72. Saanila, V., et al., *Atomic Layer Epitaxy Growth of BaS and BaS:Ce Thin Films from In Situ Synthesized Ba(thd)2.* Chemical Vapor Deposition, 1998. **4**(6): p. 227-233.
73. Ihanus, J., et al., *Blue- and green-emitting SrS:Cu electroluminescent devices deposited by the atomic layer deposition technique.* Journal of Applied Physics, 2003. **94**(6): p. 3862-3868.
74. Li, W.-M., et al., *Photo- and electroluminescence of SrS:Cu and SrS:Ag,Cu,Ga thin films.* Journal of Applied Physics, 1999. **86**(9): p. 5017-5025.
75. Heikkinen, H., et al., *An XPS study of SrS:Ce thin films for electroluminescent devices.* Applied Surface Science, 1998. **133**(3): p. 205-212.
76. Benalloul, P., et al., *Ce^{3+} luminescent centres in atomic layer epitaxy SrS thin film electroluminescent devices.* The European Physical Journal - Applied Physics, 2000. **9**(01): p. 19-24.
77. Ihanus, J., et al., *Electroluminescent SrS and BaS Thin Films Deposited by ALD Using Cyclopentadienyl Precursors.* Journal of The Electrochemical Society, 2004. **151**(10): p. H221-H225.
78. Yun, S.J., Y.S. Kim, and S.-H.K. Park, *Fabrication of CaS:Pb blue phosphor by incorporating dimeric Pb^{2+} luminescent centers.* Applied Physics Letters, 2001. **78**(6): p. 721-723.
79. Asplund, M., et al., *Photoluminescence study of Tb^{3+} doped alkaline earth sulfide thin films.* Inorganica Chimica Acta, 1987. **139**(1–2): p. 261-263.
80. Ihanus, J., et al., *XPS and electroluminescence studies on $SrS_{1-x}Se_x$ and $ZnS_{1-x}Se_x$ thin films deposited by atomic layer deposition technique.* Journal of Crystal Growth, 2004. **260**(3–4): p. 440-446.
81. Terai, Y., S. Kuroda, and K. Takita, *Growth of self-organized dots of $Cd_{1-x}Mn_xTe$ on ZnTe by atomic layer epitaxy.* Journal of Crystal Growth, 2000. **214–215**(0): p. 178-182.
82. Tang, X., et al., *Growth and characterization of CdSe:Mn quantum dots.* Journal of Crystal Growth, 2003. **251**(1–4): p. 586-590.
83. Hernández-Calderón, I., M. García-Rocha, and P. Díaz-Arencibia, *Growth and characterization of ultra-thin quantum wells of II–VI semiconductors for optoelectronic applications.* physica status solidi (b), 2004. **241**(3): p. 558-563.
84. Huang, Y., J.-H. Ryou, and R.D. Dupuis, *Incorporation of indium and gallium in atomic layer epitaxy of InGaAs on InP substrates.* Journal of Crystal Growth, 2011. **321**(1): p. 60-64.

85. Mukai, K., N. Ohtsuka, and M. Sugawara, *High photoluminescence efficiency of InGaAs/GaAs quantum dots self-formed by atomic layer epitaxy technique.* Applied Physics Letters, 1997. **70**(18): p. 2416-2418.
86. Park, Y.M., et al., *Electrical and optical characterizations of self-assembled quantum dots formed by the atomic layer epitaxy technique.* Journal of Applied Physics, 2004. **95**(1): p. 123-127.
87. Michael, C.P., et al., *Growth, processing, and optical properties of epitaxial Er_2O_3 on silicon.* Opt. Express, 2008. **16**(24): p. 19649-19666.
88. Hoang, J., et al., *Optical properties of Y_2O_3 thin films doped with spatially controlled Er^{3+} by atomic layer deposition.* Journal of Applied Physics, 2007. **101**(12): p. 123116.
89. Hoang, J., et al., *Er^{3+} interlayer energy migration as the limiting photoluminescence quenching factor in nanostructured Er^{3+}:Y_2O_3 thin films.* Journal of Applied Physics, 2012. **112**(2): p. 023116-6.
90. Hoang, J., et al., *The effects of energy transfer on the Er^{3+} 1.54 μm luminescence in nanostructured Y_2O_3 thin films with heterogeneously distributed Yb^{3+} and Er^{3+} codopants.* Journal of Applied Physics, 2012. **112**(6): p. 063117-11.
91. Dingemans, G., et al., *Er^{3+} and Si luminescence of atomic layer deposited Er-doped Al_2O_3 thin films on Si(100).* Journal of Applied Physics, 2011. **109**(11): p. 113107.
92. Aaltonen, T., et al., *Lanthanum titanate and lithium lanthanum titanate thin films grown by atomic layer deposition.* Journal of Materials Chemistry, 2010. **20**(14): p. 2877-2881.
93. Xu, R. and C.G. Takoudis, *Atomic Layer Deposition and Characterization of Amorphous $Er_xTi_{1-x}O_y$ Dielectric Ultra-Thin Films.* ECS Journal of Solid State Science and Technology, 2012. **1**(6): p. N107-N114.
94. Rocha, L.A., et al., *Eu (III) as a probe in titania thin films: The effect of temperature.* Materials Chemistry and Physics, 2007. **101**(1): p. 238-241.
95. García-Macedo, J.A., G. Valverde-Aguilar, and S. Flores-Duran, *Eu^{3+} as optical probe of the structure in amorphous and nanocrystalline TiO_2 films prepared by sol-gel method.* 2010: p. 775503-775503.
96. Palomino-Merino, R., et al., *Photoluminescence of TiO_2: Eu^{3+} thin films obtained by sol–gel on Si and Corning glass substrates.* Thin Solid Films, 2001. **401**(1–2): p. 118-123.
97. Nebatti, A., et al., *Sol–gel-deposition of thin TiO_2:Eu^{3+} thermographic phosphor films.* Progress in Organic Coatings, 2010. **67**(3): p. 356-360.
98. Jia, C.W., et al., *Visible and near-infrared photoluminescences of europium-doped titania film.* Journal of Applied Physics, 2006. **100**(2): p. 023529-5.

99. Leroy, C., et al., *Sol–gel technique for the generation of europium-doped mesoporous and dense thin films: A luminescent study.* Journal of Luminescence, 2009. **129**(12): p. 1641-1645.
100. Chen, B.J., et al., *Optical properties of Eu^{3+} in transparent Y–Ti–O nanocrystallized sol–gel film.* Journal of Alloys and Compounds, 2009. **485**(1–2): p. L5-L8.
101. Johannsen, S.R., et al., *Optimization of Er^{3+}-doped TiO_2-thin films for infrared light up-conversion.* Thin Solid Films, 2014. **550**(0): p. 499-503.
102. Mao, X., et al., *Up-conversion fluorescence characteristics and mechanism of Er^{3+}-doped TiO_2 thin films.* Vacuum, 2014. **102**(0): p. 38-42.
103. Huang, S.-H., *Effects of Eu^{3+} and Er^{3+} Doping on Photoelectrical Performance of Dye-Sensitized Solar Cells.* Journal of the American Ceramic Society, 2013. **96**(10): p. 3108-3113.
104. Jenouvrier, P., et al., *Influence of crystallisation on the photoluminescence properties of $Y_{2-x}Er_xTi_2O_7$ sol-gel thin films.* Applied Physics A, 2003. **77**(5): p. 687-692.
105. Sheng, Y., et al., *Photoluminescence of TiO_2 films co-doped with Tb^{3+}/ $Gd^{3+}$and energy transfer from TiO_2/Gd^{3+} to Tb^{3+} ions.* Thin Solid Films, 2011. **519**(22): p. 7966-7970.
106. Jenouvrier, P., et al., *Up-conversion emission in rare earth-doped $Y_2Ti_2O_7$ sol–gel thin films.* Journal of Luminescence, 2005. **113**(3–4): p. 291-300.
107. Frindell, K.L., et al., *Visible and near-IR luminescence via energy transfer in rare earth doped mesoporous titania thin films with nanocrystalline walls.* Journal of Solid State Chemistry, 2003. **172**(1): p. 81-88.
108. Gaponenko, N.V., et al., *Photoluminescence of Eu-doped titania xerogel spin-on deposited on porous anodic alumina.* Sensors and Actuators A: Physical, 2002. **99**(1-2): p. 71-73.
109. Leroy, C.M., et al., *Europium-Doped Mesoporous Titania Thin Films: Rare-Earth Locations and Emission Fluctuations under Illumination.* ChemPhysChem, 2008. **9**(14): p. 2077-2084.
110. Forissier, S., et al., *Thulium and ytterbium-doped titania thin films deposited by MOCVD.* Energy Procedia, 2011. **10**(0): p. 192-196.
111. Hafez, H., M. Saif, and M.S.A. Abdel-Mottaleb, *Down-converting lanthanide doped TiO_2 photoelectrodes for efficiency enhancement of dye-sensitized solar cells.* Journal of Power Sources, 2011. **196**(13): p. 5792-5796.
112. Oja Acik, I., et al., *Characterisation of samarium and nitrogen co-doped TiO_2 films prepared by chemical spray pyrolysis.* Applied Surface Science, 2012. **261**(0): p. 735-741.

113. Le Boulbar, E., et al., *Optical properties of rare earth-doped TiO_2 anatase and rutile thin films grown by pulsed-laser deposition.* Thin Solid Films, 2014. **553**(0): p. 13-16.
114. Brixner, L.H., *Preparation and Properties of the $Ln_2Ti_2O_7$-Type Rare Earth Titanate.* Inorganic Chemistry, 1964. **3**(7): p. 1065-1067.
115. Blasse, G., A. Bril, and W.C. Nieuwpoort, *On the Eu^{3+} fluorescence in mixed metal oxides: Part I—The crystal structure sensitivity of the intensity ratio of electric and magnetic dipole emission.* Journal of Physics and Chemistry of Solids, 1966. **27**(10): p. 1587-1592.
116. Ovenstone, J., et al., *A Study of the Effects of Europium Doping and Calcination on the Luminescence of Titania Phosphor Materials.* The Journal of Physical Chemistry B, 2001. **105**(30): p. 7170-7177.
117. Ovenstone, J., et al., *Luminescence in europium-doped titania: Part II. High concentration range of Eu^{3+}.* Journal of Materials Research, 2002. **17**(10): p. 2524-2531.
118. Cheng, H., et al., *Sol-gel synthesis and photoluminescence characterization of $La_2Ti_2O_7:Eu^{3+}$ nanocrystals.* Rare Metals, 2011. **30**(6): p. 602-606.

I

Paper I

Structural and optical properties of lanthanide oxides grown by atomic layer deposition (Ln = Pr, Nd, Sm, Eu, Tb, Dy, Ho, Er, Tm, Yb)

Per-Anders Hansen, Helmer Fjellvåg, Terje Finstad and Ola Nilsen

Dalton Transactions, 2013, issue 42, page 10778-10785

Paper II

II

Luminescence properties of europium titanate thin films grown by atomic layer deposition

Per-Anders Hansen, Helmer Fjellvåg, Terje Finstad and Ola Nilsen

RSC Advances, 2014, issue 23, page 11876-11883

Paper III

Luminescence of multilayered Eu_2O_3 and TiO_2 grown by atomic layer deposition

Per-Anders Hansen, Helmer Fjellvåg, Terje Finstad and Ola Nilsen

Submitted to Journal of Chemical Vapor Deposition for an ALD special issue, review pending.

III

Paper IV

Luminescence properties of lanthanide titanate and lanthanide ytterbium titanate thin films grown by atomic layer deposition

Per-Anders Hansen, Helmer Fjellvåg, Terje Finstad and Ola Nilsen

Manuscript draft, to be submitted.

IV